



CHORUS

This is the accepted manuscript made available via CHORUS. The article has been published as:

Measurement of $Y(1S+2S+3S)$ production in p+p and Au + Au collisions at $\sqrt{s_{NN}}=200$ GeV

A. Adare *et al.* (PHENIX Collaboration)

Phys. Rev. C **91**, 024913 — Published 24 February 2015

DOI: [10.1103/PhysRevC.91.024913](https://doi.org/10.1103/PhysRevC.91.024913)

1 Measurement of $\Upsilon(1S+2S+3S)$ production in p+p and Au+Au collisions at $\sqrt{s_{NN}} = 200$
2 GeV

3 A. Adare,¹⁴ S. Afanasiev,³² C. Aidala,^{41,45,46} N.N. Ajitanand,⁶⁵ Y. Akiba,^{59,60} R. Akimoto,¹³ H. Al-Bataineh,⁵³
4 H. Al-Ta'ani,⁵³ J. Alexander,⁶⁵ A. Angerami,¹⁵ K. Aoki,^{37,59} N. Apadula,⁶⁶ L. Aphecetche,⁶⁷ Y. Aramaki,^{13,59}
5 J. Asai,⁵⁹ H. Asano,^{37,59} E.C. Aschenauer,⁸ E.T. Atomssa,^{38,66} R. Averbeck,⁶⁶ T.C. Awes,⁵⁵ B. Azmoun,⁸
6 V. Babintsev,²⁶ M. Bai,⁷ G. Baksay,²¹ L. Baksay,²¹ A. Baldisseri,¹⁷ B. Bannier,⁶⁶ K.N. Barish,⁹ P.D. Barnes,^{41,*}
7 B. Bassalleck,⁵² A.T. Basye,¹ S. Bathe,^{6,9,60} S. Batsouli,⁵⁵ V. Baublis,⁵⁸ C. Baumann,⁴⁷ S. Baumgart,⁵⁹
8 A. Bazilevsky,⁸ S. Belikov,^{8,*} R. Belmont,⁷¹ R. Bennett,⁶⁶ A. Berdnikov,⁶² Y. Berdnikov,⁶² A.A. Bickley,¹⁴
9 X. Bing,⁵⁴ D.S. Blau,³⁶ J.G. Boissevain,⁴¹ J.S. Bok,⁵³ H. Borel,¹⁷ K. Boyle,^{60,66} M.L. Brooks,⁴¹ H. Buesching,⁸
10 V. Bumazhnov,²⁶ G. Bunce,^{8,60} S. Butsyk,^{41,52} C.M. Camacho,⁴¹ S. Campbell,⁶⁶ P. Castera,⁶⁶ B.S. Chang,⁷⁵
11 W.C. Chang,² J.-L. Charvet,¹⁷ C.-H. Chen,⁶⁶ S. Chernichenko,²⁶ C.Y. Chi,¹⁵ M. Chiu,^{8,27} I.J. Choi,^{27,75}
12 J.B. Choi,¹¹ S. Choi,⁶⁴ R.K. Choudhury,⁵ P. Christiansen,⁴³ T. Chujo,⁷⁰ P. Chung,⁶⁵ A. Churnin,²⁶ O. Chvala,⁹
13 V. Cianciolo,⁵⁵ Z. Citron,⁶⁶ B.A. Cole,¹⁵ M. Connors,⁶⁶ P. Constantin,⁴¹ M. Csanád,¹⁹ T. Csörgő,⁷⁴ T. Dahms,⁶⁶
14 S. Dairaku,^{37,59} K. Das,²² A. Datta,⁴⁵ M.S. Daugherty,¹ G. David,⁸ A. Denisov,²⁶ D. d'Enterria,³⁸
15 A. Deshpande,^{60,66} E.J. Desmond,⁸ K.V. Dharmawardane,⁵³ O. Dietzsch,⁶³ L. Ding,³⁰ A. Dion,^{30,66} M. Donadelli,⁶³
16 O. Drapier,³⁸ A. Drees,⁶⁶ K.A. Drees,⁷ A.K. Dubey,⁷³ J.M. Durham,^{41,66} A. Durum,²⁶ D. Dutta,⁵
17 V. Dzhordzhadze,⁹ L. D'Orazio,⁴⁴ S. Edwards,⁷ Y.V. Efremenko,⁵⁵ F. Ellinghaus,¹⁴ T. Engelmores,¹⁵
18 A. Enokizono,^{40,55} H. En'yo,^{59,60} S. Esumi,⁷⁰ K.O. Eyster,⁹ B. Fadem,⁴⁸ D.E. Fields,^{52,60} M. Finger,¹⁰
19 M. Finger, Jr.,¹⁰ F. Fleuret,³⁸ S.L. Fokin,³⁶ Z. Fraenkel,^{73,*} J.E. Frantz,^{54,66} A. Franz,⁸ A.D. Frawley,²²
20 K. Fujiwara,⁵⁹ Y. Fukao,^{37,59} T. Fusayasu,⁵⁰ K. Gainey,¹ C. Gal,⁶⁶ A. Garishvili,⁶⁸ I. Garishvili,^{40,68} A. Glenn,^{14,40}
21 H. Gong,⁶⁶ X. Gong,⁶⁵ M. Gonin,³⁸ J. Gosset,¹⁷ Y. Goto,^{59,60} R. Granier de Cassagnac,³⁸ N. Grau,^{3,15}
22 S.V. Greene,⁷¹ M. Grosse Perdekamp,^{27,60} T. Gunji,¹³ L. Guo,⁴¹ H.-Å. Gustafsson,^{43,*} T. Hachiya,⁵⁹
23 A. Hadj Henni,⁶⁷ J.S. Haggerty,⁸ K.I. Hahn,²⁰ H. Hamagaki,¹³ R. Han,⁵⁷ J. Hanks,¹⁵ E.P. Hartouni,⁴⁰ K. Haruna,²⁵
24 K. Hashimoto,^{59,61} E. Haslum,⁴³ R. Hayano,¹³ X. He,²³ M. Heffner,⁴⁰ T.K. Hemmick,⁶⁶ T. Hester,⁹ J.C. Hill,³⁰
25 M. Hohlmann,²¹ R.S. Hollis,⁹ W. Holzmann,⁶⁵ K. Homma,²⁵ B. Hong,³⁵ T. Horaguchi,^{13,59,69,70} Y. Hori,¹³
26 D. Hornback,⁶⁸ S. Huang,⁷¹ T. Ichihara,^{59,60} R. Ichimiya,⁵⁹ H. Iinuma,^{34,37,59} Y. Ikeda,^{59,70} K. Imai,^{31,37,59}
27 J. Imrek,¹⁸ M. Inaba,⁷⁰ A. Iordanova,⁹ D. Isenhower,¹ M. Ishihara,⁵⁹ T. Isobe,^{13,59} M. Issah,^{65,71} A. Isupov,³²
28 D. Ivanischev,⁵⁸ D. Ivanishchev,⁵⁸ B.V. Jacak,⁶⁶ M. Javani,²³ J. Jia,^{8,15,65} X. Jiang,⁴¹ J. Jin,¹⁵ B.M. Johnson,⁸
29 K.S. Joo,⁴⁹ D. Jouan,⁵⁶ D.S. Jumper,²⁷ F. Kajihara,¹³ S. Kametani,⁵⁹ N. Kamihara,⁶⁰ J. Kamin,⁶⁶ S. Kaneti,⁶⁶
30 B.H. Kang,²⁴ J.H. Kang,⁷⁵ J.S. Kang,²⁴ J. Kapustinsky,⁴¹ K. Karatsu,^{37,59} M. Kasai,^{59,61} D. Kawall,^{45,60}
31 A.V. Kazantsev,³⁶ T. Kempel,³⁰ A. Khanzadeev,⁵⁸ K.M. Kijima,²⁵ J. Kikuchi,⁷² B.I. Kim,³⁵ C. Kim,³⁵ D.H. Kim,⁴⁹
32 D.J. Kim,^{33,75} E. Kim,⁶⁴ E.-J. Kim,¹¹ H.-J. Kim,⁷⁵ K.-B. Kim,¹¹ S.H. Kim,⁷⁵ Y.-J. Kim,²⁷ Y.K. Kim,²⁴ E. Kinney,¹⁴
33 K. Kiriluk,¹⁴ Á. Kiss,¹⁹ E. Kistenev,⁸ J. Klatsky,²² J. Klay,⁴⁰ C. Klein-Boesing,⁴⁷ D. Kleinjan,⁹ P. Kline,⁶⁶
34 L. Kochenda,⁵⁸ Y. Komatsu,¹³ B. Komkov,⁵⁸ M. Konno,⁷⁰ J. Koster,²⁷ D. Kotchetkov,⁵⁴ D. Kotov,^{58,62}
35 A. Kozlov,⁷³ A. Král,¹⁶ A. Kravitz,¹⁵ F. Krizek,³³ G.J. Kunde,⁴¹ K. Kurita,^{59,61} M. Kurosawa,⁵⁹ M.J. Kweon,³⁵
36 Y. Kwon,^{68,75} G.S. Kyle,⁵³ R. Lacey,⁶⁵ Y.S. Lai,¹⁵ J.G. Lajoie,³⁰ D. Layton,²⁷ A. Lebedev,³⁰ B. Lee,²⁴ D.M. Lee,⁴¹
37 J. Lee,²⁰ K.B. Lee,³⁵ K.S. Lee,³⁵ S.H. Lee,⁶⁶ S.R. Lee,¹¹ T. Lee,⁶⁴ M.J. Leitch,⁴¹ M.A.L. Leite,⁶³ M. Leitgab,²⁷
38 B. Lenzi,⁶³ B. Lewis,⁶⁶ X. Li,¹² P. Liebing,⁶⁰ S.H. Lim,⁷⁵ L.A. Linden Levy,¹⁴ T. Liška,¹⁶ A. Litvinenko,³²
39 H. Liu,⁵³ M.X. Liu,⁴¹ B. Love,⁷¹ D. Lynch,⁸ C.F. Maguire,⁷¹ Y.I. Makdisi,⁷ M. Makek,^{73,76} A. Malakhov,³²
40 M.D. Malik,⁵² A. Manion,⁶⁶ V.I. Manko,³⁶ E. Mannel,¹⁵ Y. Mao,^{57,59} L. Mašek,^{10,29} H. Masui,⁷⁰ S. Masumoto,¹³
41 F. Matathias,¹⁵ M. McCumber,^{14,66} P.L. McGaughey,⁴¹ D. McGlinchey,^{14,22} C. McKinney,²⁷ N. Means,⁶⁶
42 M. Mendoza,⁹ B. Meredith,²⁷ Y. Miake,⁷⁰ T. Mibe,³⁴ A.C. Mignerey,⁴⁴ P. Mikeš,²⁹ K. Miki,⁷⁰ A. Milov,^{8,73}
43 D.K. Mishra,⁵ M. Mishra,⁴ J.T. Mitchell,⁸ Y. Miyachi,^{59,69} S. Miyasaka,^{59,69} A.K. Mohanty,⁵ H.-J. Moon,⁴⁹
44 Y. Morino,¹³ A. Morreale,⁹ D.P. Morrison,^{8,†} S. Motschwiller,⁴⁸ T.V. Moukhanova,³⁶ D. Mukhopadhyay,⁷¹
45 T. Murakami,^{37,59} J. Murata,^{59,61} T. Nagae,³⁷ S. Nagamiya,^{34,59} J.L. Nagle,^{14,‡} M. Naglis,⁷³ M.I. Nagy,^{19,74}
46 I. Nakagawa,^{59,60} Y. Nakamiya,²⁵ K.R. Nakamura,^{37,59} T. Nakamura,^{25,59} K. Nakano,^{59,69} C. Nattrass,⁶⁸
47 A. Nederlof,⁴⁸ J. Newby,⁴⁰ M. Nguyen,⁶⁶ M. Nishida,^{25,59} T. Niida,⁷⁰ R. Nouicer,^{8,60} N. Novitzky,³³ A.S. Nyanin,³⁶
48 E. O'Brien,⁸ S.X. Oda,¹³ C.A. Ogilvie,³⁰ M. Oka,⁷⁰ K. Okada,⁶⁰ Y. Onuki,⁵⁹ A. Oskarsson,⁴³ M. Ouchida,^{25,59}
49 K. Ozawa,¹³ R. Pak,⁸ A.P.T. Palounek,⁴¹ V. Pantuev,^{28,66} V. Papavassiliou,⁵³ B.H. Park,²⁴ I.H. Park,²⁰
50 J. Park,⁶⁴ S.K. Park,³⁵ W.J. Park,³⁵ S.F. Pate,⁵³ L. Patel,²³ H. Pei,³⁰ J.-C. Peng,²⁷ H. Pereira,¹⁷ V. Peresedov,³²
51 D.Yu. Peressounko,³⁶ R. Petti,^{8,66} C. Pinkenburg,⁸ R.P. Pisani,⁸ M. Proissl,⁶⁶ M.L. Purschke,⁸ A.K. Purwar,⁴¹
52 H. Qu,^{1,23} J. Rak,^{33,52} A. Rakotozafindrabe,³⁸ I. Ravinovich,⁷³ K.F. Read,^{55,68} S. Rembeczki,²¹ K. Reygers,⁴⁷

53 D. Reynolds,⁶⁵ V. Riabov,⁵⁸ Y. Riabov,^{58,62} E. Richardson,⁴⁴ N. Riveli,⁵⁴ D. Roach,⁷¹ G. Roche,⁴² S.D. Rolnick,⁹
 54 M. Rosati,³⁰ S.S.E. Rosendahl,⁴³ P. Rosnet,⁴² P. Rukoyatkin,³² P. Ružička,²⁹ V.L. Rykov,⁵⁹ B. Sahlmueller,^{47,66}
 55 N. Saito,^{34,37,59,60} T. Sakaguchi,⁸ S. Sakai,⁷⁰ K. Sakashita,^{59,69} V. Samsonov,^{51,58} M. Sano,⁷⁰ M. Sarsour,²³
 56 T. Sato,⁷⁰ S. Sawada,³⁴ K. Sedgwick,⁹ J. Seele,¹⁴ R. Seidl,^{27,59,60} A.Yu. Semenov,³⁰ V. Semenov,^{26,28} A. Sen,²³
 57 R. Seto,⁹ D. Sharma,⁷³ I. Shein,²⁶ T.-A. Shibata,^{59,69} K. Shigaki,²⁵ M. Shimomura,⁷⁰ K. Shoji,^{37,59} P. Shukla,⁵
 58 A. Sickles,⁸ C.L. Silva,^{30,63} D. Silvermyr,⁵⁵ C. Silvestre,¹⁷ K.S. Sim,³⁵ B.K. Singh,⁴ C.P. Singh,⁴ V. Singh,⁴
 59 M. Slunečka,¹⁰ A. Soldatov,²⁶ R.A. Soltz,⁴⁰ W.E. Sondheim,⁴¹ S.P. Sorensen,⁶⁸ M. Soumya,⁶⁵ I.V. Sourikova,⁸
 60 F. Staley,¹⁷ P.W. Stankus,⁵⁵ E. Stenlund,⁴³ M. Stepanov,^{45,53} A. Ster,⁷⁴ S.P. Stoll,⁸ T. Sugitate,²⁵ C. Suire,⁵⁶
 61 A. Sukhanov,⁸ J. Sun,⁶⁶ J. Sziklai,⁷⁴ E.M. Takagui,⁶³ A. Takahara,¹³ A. Taketani,^{59,60} R. Tanabe,⁷⁰ Y. Tanaka,⁵⁰
 62 S. Taneja,⁶⁶ K. Tanida,^{59,60,64} M.J. Tannenbaum,⁸ S. Tarafdar,⁴ A. Taranenko,^{51,65} P. Tarján,¹⁸ E. Tennant,⁵³
 63 H. Themann,⁶⁶ T.L. Thomas,⁵² T. Todoroki,^{59,70} M. Togawa,^{37,59} A. Toia,⁶⁶ L. Tomášek,²⁹ M. Tomášek,^{16,29}
 64 Y. Tomita,⁷⁰ H. Torii,^{25,59} R.S. Towell,¹ V.-N. Tram,³⁸ I. Tserruya,⁷³ Y. Tsuchimoto,^{13,25} T. Tsuji,¹³ C. Vale,^{8,30}
 65 H. Valle,⁷¹ H.W. van Hecke,⁴¹ M. Vargyas,¹⁹ E. Vazquez-Zambrano,¹⁵ A. Veicht,^{15,27} J. Velkovska,⁷¹ R. Vértesi,^{18,74}
 66 A.A. Vinogradov,³⁶ M. Virius,¹⁶ A. Vossen,²⁷ V. Vrba,^{16,29} E. Vznuzdaev,⁵⁸ X.R. Wang,⁵³ D. Watanabe,²⁵
 67 K. Watanabe,⁷⁰ Y. Watanabe,^{59,60} Y.S. Watanabe,¹³ F. Wei,³⁰ R. Wei,⁶⁵ J. Wessels,⁴⁷ S. Whitaker,³⁰
 68 S.N. White,⁸ D. Winter,¹⁵ S. Wolin,²⁷ C.L. Woody,⁸ M. Wysocki,¹⁴ W. Xie,⁶⁰ Y.L. Yamaguchi,^{13,59,72}
 69 K. Yamaura,²⁵ R. Yang,²⁷ A. Yanovich,²⁶ J. Ying,²³ S. Yokkaichi,^{59,60} Z. You,⁴¹ G.R. Young,⁵⁵ I. Younus,^{39,52}
 70 I.E. Yushmanov,³⁶ W.A. Zajc,¹⁵ O. Zaudtke,⁴⁷ A. Zelenski,⁷ C. Zhang,⁵⁵ S. Zhou,¹² and L. Zolin³²

(PHENIX Collaboration)

¹Abilene Christian University, Abilene, Texas 79699, USA

²Institute of Physics, Academia Sinica, Taipei 11529, Taiwan

³Department of Physics, Augustana College, Sioux Falls, South Dakota 57197, USA

⁴Department of Physics, Banaras Hindu University, Varanasi 221005, India

⁵Bhabha Atomic Research Centre, Bombay 400 085, India

⁶Baruch College, City University of New York, New York, New York, 10010 USA

⁷Collider-Accelerator Department, Brookhaven National Laboratory, Upton, New York 11973-5000, USA

⁸Physics Department, Brookhaven National Laboratory, Upton, New York 11973-5000, USA

⁹University of California - Riverside, Riverside, California 92521, USA

¹⁰Charles University, Ovocný trh 5, Praha 1, 116 36, Prague, Czech Republic

¹¹Chonbuk National University, Jeonju, 561-756, Korea

¹²Science and Technology on Nuclear Data Laboratory, China Institute of Atomic Energy, Beijing 102413, P. R. China

¹³Center for Nuclear Study, Graduate School of Science, University of Tokyo, 7-3-1 Hongo, Bunkyo, Tokyo 113-0033, Japan

¹⁴University of Colorado, Boulder, Colorado 80309, USA

¹⁵Columbia University, New York, New York 10027 and Nevis Laboratories, Irvington, New York 10533, USA

¹⁶Czech Technical University, Žitkova 4, 166 36 Prague 6, Czech Republic

¹⁷Dapnia, CEA Saclay, F-91191, Gif-sur-Yvette, France

¹⁸Debrecen University, H-4010 Debrecen, Egyetem tér 1, Hungary

¹⁹ELTE, Eötvös Loránd University, H - 1117 Budapest, Pázmány P. s. 1/A, Hungary

²⁰Ewha Womans University, Seoul 120-750, Korea

²¹Florida Institute of Technology, Melbourne, Florida 32901, USA

²²Florida State University, Tallahassee, Florida 32306, USA

²³Georgia State University, Atlanta, Georgia 30303, USA

²⁴Hanyang University, Seoul 133-792, Korea

²⁵Hiroshima University, Kagamiyama, Higashi-Hiroshima 739-8526, Japan

²⁶IHEP Protvino, State Research Center of Russian Federation, Institute for High Energy Physics, Protvino, 142281, Russia

²⁷University of Illinois at Urbana-Champaign, Urbana, Illinois 61801, USA

²⁸Institute for Nuclear Research of the Russian Academy of Sciences, prospekt 60-letiya Oktyabrya 7a, Moscow 117312, Russia

²⁹Institute of Physics, Academy of Sciences of the Czech Republic, Na Slovance 2, 182 21 Prague 8, Czech Republic

³⁰Iowa State University, Ames, Iowa 50011, USA

³¹Advanced Science Research Center, Japan Atomic Energy Agency, 2-4

Shirakata Shirane, Tokai-mura, Naka-gun, Ibaraki-ken 319-1195, Japan

³²Joint Institute for Nuclear Research, 141980 Dubna, Moscow Region, Russia

³³Helsinki Institute of Physics and University of Jyväskylä, P.O.Box 35, FI-40014 Jyväskylä, Finland

³⁴KEK, High Energy Accelerator Research Organization, Tsukuba, Ibaraki 305-0801, Japan

³⁵Korea University, Seoul, 136-701, Korea

³⁶Russian Research Center "Kurchatov Institute", Moscow, 123098 Russia

³⁷Kyoto University, Kyoto 606-8502, Japan

³⁸Laboratoire Leprince-Ringuet, Ecole Polytechnique, CNRS-IN2P3, Route de Saclay, F-91128, Palaiseau, France

³⁹Physics Department, Lahore University of Management Sciences, Lahore 54792, Pakistan

⁴⁰Lawrence Livermore National Laboratory, Livermore, California 94550, USA

- 113 ⁴¹ Los Alamos National Laboratory, Los Alamos, New Mexico 87545, USA
 114 ⁴² LPC, Université Blaise Pascal, CNRS-IN2P3, Clermont-Fd, 63177 Aubiere Cedex, France
 115 ⁴³ Department of Physics, Lund University, Box 118, SE-221 00 Lund, Sweden
 116 ⁴⁴ University of Maryland, College Park, Maryland 20742, USA
 117 ⁴⁵ Department of Physics, University of Massachusetts, Amherst, Massachusetts 01003-9337, USA
 118 ⁴⁶ Department of Physics, University of Michigan, Ann Arbor, Michigan 48109-1040, USA
 119 ⁴⁷ Institut für Kernphysik, University of Muenster, D-48149 Muenster, Germany
 120 ⁴⁸ Muhlenberg College, Allentown, Pennsylvania 18104-5586, USA
 121 ⁴⁹ Myongji University, Yongin, Kyonggido 449-728, Korea
 122 ⁵⁰ Nagasaki Institute of Applied Science, Nagasaki-shi, Nagasaki 851-0193, Japan
 123 ⁵¹ National Research Nuclear University, MEPhI, Moscow Engineering Physics Institute, Moscow, 115409, Russia
 124 ⁵² University of New Mexico, Albuquerque, New Mexico 87131, USA
 125 ⁵³ New Mexico State University, Las Cruces, New Mexico 88003, USA
 126 ⁵⁴ Department of Physics and Astronomy, Ohio University, Athens, Ohio 45701, USA
 127 ⁵⁵ Oak Ridge National Laboratory, Oak Ridge, Tennessee 37831, USA
 128 ⁵⁶ IPN-Orsay, Université Paris Sud, CNRS-IN2P3, BP1, F-91406, Orsay, France
 129 ⁵⁷ Peking University, Beijing 100871, P. R. China
 130 ⁵⁸ PNPI, Petersburg Nuclear Physics Institute, Gatchina, Leningrad region, 188300, Russia
 131 ⁵⁹ RIKEN Nishina Center for Accelerator-Based Science, Wako, Saitama 351-0198, Japan
 132 ⁶⁰ RIKEN BNL Research Center, Brookhaven National Laboratory, Upton, New York 11973-5000, USA
 133 ⁶¹ Physics Department, Rikkyo University, 3-34-1 Nishi-Ikebukuro, Toshima, Tokyo 171-8501, Japan
 134 ⁶² Saint Petersburg State Polytechnic University, St. Petersburg, 195251 Russia
 135 ⁶³ Universidade de São Paulo, Instituto de Física, Caixa Postal 66318, São Paulo CEP05315-970, Brazil
 136 ⁶⁴ Department of Physics and Astronomy, Seoul National University, Seoul 151-742, Korea
 137 ⁶⁵ Chemistry Department, Stony Brook University, SUNY, Stony Brook, New York 11794-3400, USA
 138 ⁶⁶ Department of Physics and Astronomy, Stony Brook University, SUNY, Stony Brook, New York 11794-3800, USA
 139 ⁶⁷ SUBATECH (Ecole des Mines de Nantes, CNRS-IN2P3, Université de Nantes) BP 20722 - 44307, Nantes, France
 140 ⁶⁸ University of Tennessee, Knoxville, Tennessee 37996, USA
 141 ⁶⁹ Department of Physics, Tokyo Institute of Technology, Oh-okayama, Meguro, Tokyo 152-8551, Japan
 142 ⁷⁰ Institute of Physics, University of Tsukuba, Tsukuba, Ibaraki 305, Japan
 143 ⁷¹ Vanderbilt University, Nashville, Tennessee 37235, USA
 144 ⁷² Waseda University, Advanced Research Institute for Science and
 145 Engineering, 17 Kikui-cho, Shinjuku-ku, Tokyo 162-0044, Japan
 146 ⁷³ Weizmann Institute, Rehovot 76100, Israel
 147 ⁷⁴ Institute for Particle and Nuclear Physics, Wigner Research Centre for Physics, Hungarian
 148 Academy of Sciences (Wigner RCP, RMKI) H-1525 Budapest 114, POBox 49, Budapest, Hungary
 149 ⁷⁵ Yonsei University, IPAP, Seoul 120-749, Korea
 150 ⁷⁶ University of Zagreb, Faculty of Science, Department of Physics, Bijenička 32, HR-10002 Zagreb, Croatia

151 Measurements of bottomonium production in heavy ion and $p+p$ collisions at the Relativistic
 152 Heavy Ion Collider (RHIC) are presented. The inclusive yield of the three Υ states, $\Upsilon(1S + 2S +$
 153 $3S)$, was measured in the PHENIX experiment via electron-positron decay pairs at midrapidity for
 154 Au+Au and $p+p$ collisions at $\sqrt{s_{NN}} = 200$ GeV. The $\Upsilon(1S + 2S + 3S) \rightarrow e^+e^-$ differential cross
 155 section at midrapidity was found to be $B_{ee}d\sigma/dy = 108 \pm 38$ (stat) ± 15 (syst) ± 11 (luminosity)
 156 pb in $p+p$ collisions. The nuclear modification factor in the 30% most central Au+Au collisions
 157 indicates a suppression of the total Υ state yield relative to the extrapolation from $p+p$ collision
 158 data. The suppression is consistent with measurements made by STAR at RHIC and at higher
 159 energies by the CMS experiment at the Large Hadron Collider.

160 PACS numbers: 25.75.Dw

* Deceased

† PHENIX Co-Spokesperson: morrison@bnl.gov

‡ PHENIX Co-Spokesperson: jamie.nagle@colorado.edu

I. INTRODUCTION

161

162 One of the main physics programs in relativistic heavy ion collisions is the study of heavy quarkonia yields, namely
 163 charm quark pairs (charmonia) and bottom quark pairs (bottomonia). At zero temperature, the binding energy
 164 between the heavy quark and anti-quark ($Q\bar{Q}$) in these vector mesons may be described by an effective potential
 165 consisting of a confining term at large distance and Coulomb-like term at short distance [1].

166 When the temperature of the medium formed after the collision is higher than a transition temperature $T_c \approx 170$ MeV,
 167 the effective potential between light quark and anti-quark weakens and deconfines the constituent quarks of mesons
 168 and baryons. The Quark-Gluon Plasma (QGP) formed can be described as a dense, strongly coupled state of matter
 169 which reaches thermalization in less than 1 fm/c [2].

170 In the QGP medium, the effective color electric potential between Q and \bar{Q} can be screened by the dense surrounding
 171 color charges. This color screening is similar to the Debye screening observed in electromagnetic plasmas [3]. The
 172 temperature at which the heavy quark state becomes unbound due to this screening depends on the corresponding
 173 binding energy of the state. Because of the large variation in radii between the different heavy quarkonia, they are
 174 expected to become unbound at different temperatures.

175 There are many theoretical calculations which predict the temperature at which each quarkonium state is suppressed
 176 by color screening. A compilation of results can be found in [4], including lattice quantum chromodynamics (QCD) [5–
 177 15], QCD sum rules [4, 16–20], AdS/QCD [21–24], resummed perturbation theory [25, 26], effective field theories [27,
 178 28], and potential models [15, 29–35]. Figure 1 shows the dissociation temperature range for several quarkonium states
 179 as expected from these models. Besides the different techniques used in these calculations, the melting range also
 180 depends on the choice of the transition temperature, the use of the internal energy or the free energy of the system
 181 for the temperature dependence of the heavy quark potential and the criteria adopted for defining the dissociation
 182 point. No cold nuclear matter effects have been considered in these estimations.

183 A comparison between hydrodynamical model calculations and the PHENIX thermal photon data [36] suggests
 184 that the peak temperature of the medium formed at RHIC in central Au+Au collisions at $\sqrt{s_{NN}} = 200$ GeV lies in
 185 the region between 300 and 600 MeV, or $1.8 T_c$ and $3.5 T_c$. The majority of the estimates shown in Fig. 1 indicates
 186 that only the ground states, the J/ψ and $\Upsilon(1S)$, remain bound at these temperatures.

187 PHENIX reported a strong suppression of the J/ψ yield in central Au+Au collisions compared to binary collision
 188 scaling from $p+p$ yields [37, 38]. According to measurements performed in $p+p$ collisions at RHIC, $(42 \pm 9)\%$ of the
 189 J/ψ yield comes from χ_c and ψ' decays [39]. The complete suppression of these states in Au+Au collisions can explain
 190 only part of the suppression seen for the J/ψ . There are other possible contributions to J/ψ suppression and therefore
 191 the interpretation of the data is not straightforward. Other mechanisms of suppression include initial and final state
 192 cold nuclear matter effects, studied in $d+Au$ collisions by PHENIX [40, 41]. There are also effects that can reduce the
 193 suppression. The dissociated charm (and anti-charm) quark can undergo multiple scatterings and recombine with its
 194 former partner, once the medium cools down. In addition, the presence of about 6-20 open charm pairs in each central
 195 Au+Au collision at RHIC ¹, provides a good chance that the ground state charmonium was formed by coalescence of
 196 uncorrelated charm and anti-charm quarks present in the medium [43]. Thus, even if all the initially produced J/ψ s
 197 are dissociated in the QGP medium, J/ψ s can be re-created at a later stage by the coalescence process.

198 The probability for creating a bottomonium state through coalescence is quite small at $\sqrt{s_{NN}} = 200$ GeV, given
 199 that only about 0.07 $b\bar{b}$ pairs per central event are produced ². Therefore, bottomonium states are a better probe
 200 of color screening in Au+Au collisions at RHIC. Figure 1 shows that no lattice QCD or potential model calculation
 201 predicts that $\Upsilon(1S)$ will melt at a temperature lower than around $2 T_c$. This is an outcome of the tighter binding
 202 energy and smaller radius of the 1S state compared to other quarkonium states. Some calculations suggest the ground
 203 state charmonium is dissociated at a temperature close to T_c [20, 31, 34].

204 Bottomonia have been measured mostly in the dilepton channel with a branching ratio around 2.5% [45]. Table I
 205 lists the fraction of the three Υ states present in the dilepton spectrum as measured at Fermilab and the Large Hadron
 206 Collider (LHC) by E866/NuSea [46], CDF [47], LHCb [48] and CMS [49]. No significant variations on the relative
 207 yields have been observed in spite of the broad collision energy range of these experiments or whether the anti-proton
 208 was one of the collision particles or not. The ground state $\Upsilon(1S)$ has many feed-down contributions from excited
 209 states. The CDF experiment reported the fraction of these contributions [50], which can be seen in Table II.

210 Fermilab experiments found no modification of the relative yields in cold nuclear matter as measured in $p+d$ [46]
 211 and $p+A$ [51]. The initial state effects on bottomonia production were investigated by E605 [52], E772 [51] and
 212 E866/NuSea [46] in $p+A$ collisions at $\sqrt{s_{NN}}=38.8$ GeV with targets of ²H, C, Ca and Fe. The Υ yields are suppressed
 213 by $\sim 5\%$ for incident gluon momentum fraction $x_2 \sim 0.1$. The suppression gets stronger for larger x_2 , reaching a level of

¹ This estimation is based on the $c - \bar{c}$ total cross section reported in [42] and 1000 binary collisions in very central Au+Au events.

² Estimation based on the total $b\bar{b}$ cross section published in [44].

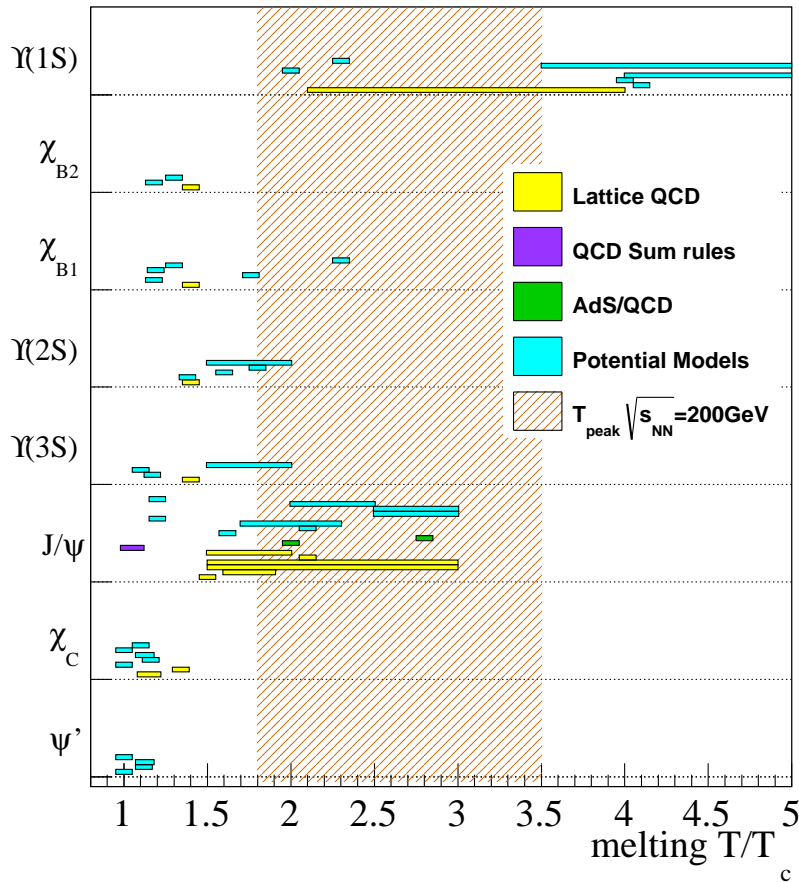


FIG. 1. (Color online) Compilation of medium temperatures relative to the critical temperature (T_c) where quarkonium states are dissociated in the quark-gluon plasma. Note that these estimations were performed assuming different T_c values. Each horizontal bar corresponds to one estimation and its temperature extension (when applied) represents the range where the quarkonia state undergoes a mass/size modification until it completely melts. Techniques used in calculations: Lattice QCD [5–15], QCD sum rules [4, 16–20], AdS/QCD [21–24], effective field theories [27, 28] and potential models [15, 29–35]. The shaded band from 1.8 to 3.5 T/T_c represents the hydrodynamic estimation for the peak temperature reached in Au+Au collisions at 200 GeV [36].

TABLE I. Composition of the Υ family in the dilepton channel as measured by E866/NuSea [46], CDF [47], LHCb [48] and CMS [49]. Fractions are in % and only statistical uncertainties are shown.

Exp.	system	$\Upsilon(1S)$	$\Upsilon(2S)$	$\Upsilon(3S)$
		$9.46 \frac{GeV}{c^2}$	$10.02 \frac{GeV}{c^2}$	$10.36 \frac{GeV}{c^2}$
E866	$p+p \sqrt{s}=39$ GeV	69.1 ± 1.0	22.2 ± 0.9	8.8 ± 0.6
CDF	$p+\bar{p} \sqrt{s}=1.8$ TeV	72.6 ± 2.8	17.6 ± 1.7	9.7 ± 1.4
LHCb	$p+p \sqrt{s}=7$ TeV	73.0 ± 0.3	17.9 ± 0.2	9.0 ± 0.2
CMS	$p+p \sqrt{s}=7$ TeV	71.6 ± 1.3	18.5 ± 0.8	10.0 ± 1.3

214 $\sim 15\%$ at $x_2 \sim 0.3$. PHENIX measured the medium modification of the Υ family (1S+2S+3S) yield in d +Au collisions
215 at $\sqrt{s_{NN}} = 200$ GeV [53]. The result is consistent with no modification within the large statistical uncertainties at
216 $x_2 \sim 10^{-2}$ and presents an one standard-deviation suppression at $x_2 \sim 0.2$, which is consistent with the Fermilab
217 results and the STAR experiment at midrapidity in d +Au collisions [54]. The RHIC results can be accounted for
218 by a combination of initial state effects, calculated by the parton modification function EPS09 [11], and quarkonium
219 breakup when crossing the cold nuclear matter.

220 QGP effects on Υ production were studied at the LHC by the CMS experiment [55] using Pb+Pb collisions at
221 $\sqrt{s_{NN}}=2.76$ TeV. The excited state $\Upsilon(2S)$ is more suppressed than the $\Upsilon(1S)$ and the $\Upsilon(3S)$ state is not seen in

TABLE II. Feed-down fractions of the $\Upsilon(1S)$ state in $p+p$ collisions as measured by CDF for $p_T > 8$ GeV/ c [50].

Source	fraction \pm stat \pm syst
Direct $\Upsilon(1S)$	$0.509 \pm 0.082 \pm 0.090$
$\Upsilon(2S)$	$0.107 \pm 0.077 \pm 0.048$
$\Upsilon(3S)$	$0.008 \pm 0.006 \pm 0.004$
χ_{B1}	$0.271 \pm 0.069 \pm 0.044$
χ_{B2}	$0.105 \pm 0.044 \pm 0.014$

222 CMS data. This is qualitatively consistent with expectations of the effects of color screening from several models
 223 discussed earlier. The question which arises is whether or not the suppression also happen at lower energies and in
 224 an environment with a much smaller number of bottom quarks present in the medium.

225 This paper reports the measurement of the inclusive Υ ($1S+2S+3S$) yield at $|y| < 0.35$ in Au+Au collisions at
 226 $\sqrt{s} = 200$ GeV. Section II describes the experimental apparatus and the data sample used in the measurement.
 227 Section III details the signal extraction, detector response and systematic uncertainties involved in this measurement.
 228 The results and comparisons with other measurements and models are presented in Section IV. The final conclusions
 229 are presented in Section V.

230 II. EXPERIMENTAL APPARATUS AND DATA SET

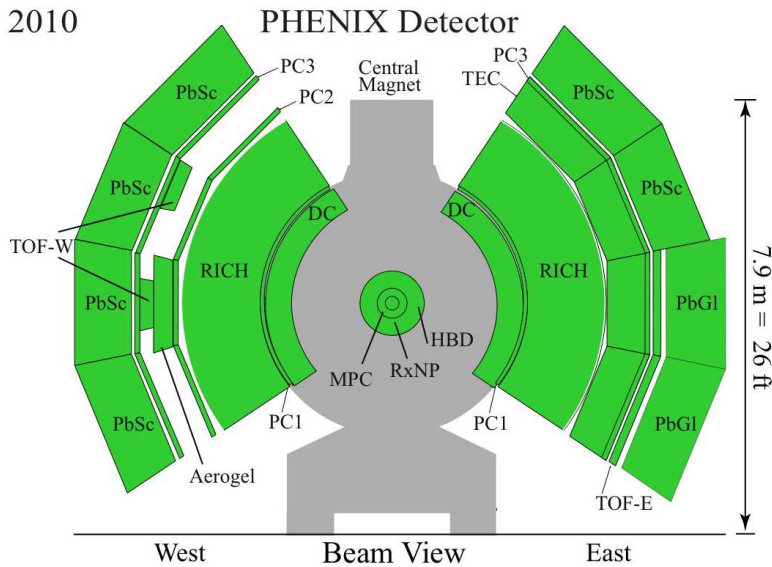


FIG. 2. (Color online) The PHENIX Central Arm Spectrometers for the 2010 data taking period.

231 The PHENIX experiment measures quarkonia at midrapidity through their dielectron decays with the two-arm
 232 central spectrometers [56] shown in Fig. 2. The central arm detectors measure electrons, photons, and hadrons over
 233 pseudorapidity of $|\eta| < 0.35$ with each arm covering azimuthal angle $\Delta\phi = \pi/2$. Charged particle tracks in the central
 234 arms are reconstructed using the drift chambers (DC), the pad chambers, and the collision point. Electron candidates
 235 are selected using information from the ring-imaging Čerenkov detector (RICH) and the electromagnetic calorimeter
 236 (EMCal) [57]. The total radiation length before the DC during the 2006 $p+p$ run was 0.4%. During the 2010 Au+Au
 237 run more material was introduced from the hadron blind detector (HBD) which added 2.4% radiation lengths to what
 238 the detector had in 2006. In the 2010 run, the magnetic field configuration was also modified to cancel the field in
 239 the HBD volume, decreasing the momentum resolution by about 25%.

240 Beam interactions were selected with a minimum bias (MB) trigger that requires at least one hit (two in Au+Au
 241 collisions) per beam crossing in each of the two beam-beam counters (BBC) placed at $3.0 < |\eta| < 3.9$. In the Au+Au
 242 data set, this was the only trigger used. A dedicated EMCal-RICH-Trigger (ERT) was used in coincidence with the

243 MB trigger during the 2006 $p+p$ data acquisition. The ERT required a minimum energy in any 2×2 group of EMCal
 244 towers, corresponding to $\Delta\eta \times \Delta\phi \approx 0.02 \times 0.02$ rad., plus associated hits in the RICH. The minimum EMCal energy
 245 requirement was 400 MeV for the first half of the run and 600 MeV for the second half.

246 The collision point along the beam direction was determined with a resolution of 1.5 cm in $p+p$ collisions and 0.5
 247 cm in Au+Au collisions, by using the difference between the time signals measured between the two BBC detectors.
 248 The collision point was required to be within ± 30 cm of the nominal center of the detector in $p+p$ collisions and ± 20
 249 cm in Au+Au collisions. The 2006 data sample was taken from $N_{pp} = 143$ billion minimum bias events, corresponding
 250 to an integrated luminosity of 6.2 pb^{-1} . The 2010 data sample was obtained from $N_{AuAu} = 5.41$ billion minimum
 251 bias events, corresponding to 0.9 nb^{-1} .

252 In $p+p$ collisions, electron candidates were identified by requiring at least one fired phototube within an annulus 3.4
 253 $< R_{\text{ring}}[\text{cm}] < 8.4$ centered in the projected track position on the RICH. The RICH is filled with a CO_2 radiator at 1
 254 atm. Pions with momentum larger than 4.8 GeV/c can also produce Čerenkov light in the RICH. Electron candidates
 255 are also required to be associated with an energy cluster in the EMCal that falls within $4\sigma_{\text{position}}$ of the projected track
 256 position and within $4\sigma_{E/p}$ of the expected energy/momentum ratio for electrons, where σ represents one standard
 257 deviation in the position and energy+momentum resolution of the EMCal+DC determined using electrons from fully
 258 reconstructed Dalitz decays. Figure 3 shows the distribution of the parameter used to select electrons in the EMCal
 259 using electron candidates used in high-mass dielectrons with $p_T > 5 \text{ GeV}/c$, above the Čerenkov threshold. Hadron
 260 contamination appears as an enhancement of this distribution for negative values. The distribution, after subtracting
 261 the background mainly composed of hadrons, represents a clean sample of electrons for $(E/p) - 1 < 4\sigma_{E/p}$.

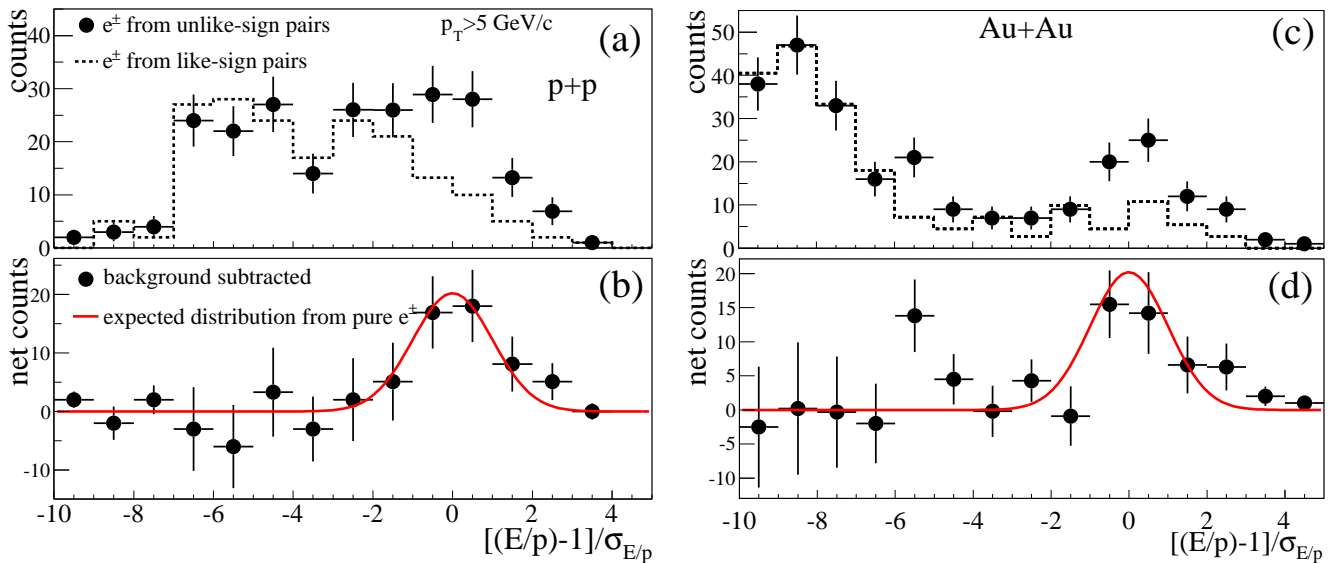


FIG. 3. (Color online) Distribution of the parameter used to identify electrons with the EMCal. E/p is the ratio between the energy deposited by the particle in the EMCal cluster and its momentum, $\sigma_{E/p}$ is the variance of the expected energy/momentum expected for electrons. The sample shown in (a) from $p+p$ collisions and (c) from Au+Au collisions is from unlike-sign electron pairs (containing signal+combinatorial background) and like-sign pairs (containing only background). (b) and (d) are the background subtracted distributions along with the expected line shape from pure electrons.

262 In the Au+Au analysis, the cuts were optimized by looking at the parameters in the detector simulations using
 263 generated $\Upsilon \rightarrow e^+e^-$ decays embedded into real data for the signal, and the real data like-sign dielectrons as a
 264 background. As a result of the optimization, we require:

- 265 • at least two fired phototubes within an annulus $3.4 < R_{\text{ring}}[\text{cm}] < 8.4$ centered in the projected track position
 266 on the RICH
- 267 • $\chi^2/npe0 < 25$, a variable defined as χ^2 -like shape of the RICH ring associated to the track over the number of
 268 photoelectrons detected in the ring
- 269 • the displacement between the ring centroid and the track projection should be smaller than 7cm
- 270 • EMCal cluster-track matching should be smaller than $3\sigma_{\text{position}}$
- 271 • EMCal cluster energy/momentum ratio should be larger than $-2.5\sigma_{E/p}$.

272 These tighter cuts allowed a better hadron rejection as can be seen in Figure 3-c compared to the $p+p$ sample in
 273 Figure 3-a.

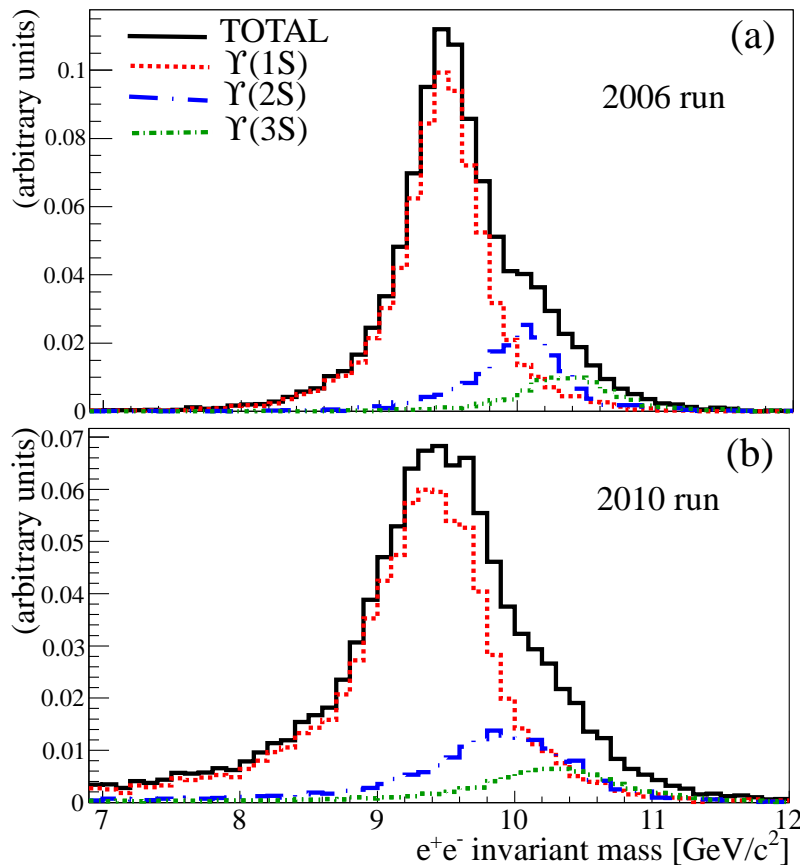


FIG. 4. (Color online) Invariant mass distribution of simulated Υ (1S+2S+3S) using the PHENIX detector simulation and relative Υ yields from CDF experiment [47] in 2006 run (a) and 2010 run (b) detector configurations.

274 Figure 4 shows the reconstructed invariant mass distribution for the three Υ states from PHENIX detector simula-
 275 tions in the 2006 $p+p$ run configuration and in 2010 Au+Au configuration. The detector is not able to separate the
 276 three states and a single peak should be observed. In the 2010 detector configuration the addition of more material
 277 in the detector introduced more bremsstrahlung for the electrons increasing the low mass tail of the peaks.

278 III. ANALYSIS PROCEDURE

279 A. Dielectrons from Υ in the Central Arms

280 The invariant mass was calculated for all electron pairs. Dielectron contributions to Υ decays are clearly identified
 281 as a peak in the unlike-sign invariant mass distributions around the Υ mass range $8.5 < M_{ee}[\text{GeV}/c^2] < 11.5$ (Fig. 5).
 282 There were 12 unlike and one like-sign dielectron within this mass region from the $p+p$ sample. In the Au+Au sample
 283 there were 22 unlike and 3 like-sign pairs in the same mass region.

284 Figure 6 shows the $p+p$ dielectron mass spectrum over an extended mass region after the like-sign distribution
 285 (used to estimate combinatorial background) has been subtracted from the unlike-sign data. Figure 7 shows the
 286 same invariant mass spectrum in the Υ mass region for $p+p$ and Au+Au data. The line shape of the Υ mass peak
 287 determined from simulations (Fig. 4) cannot be validated by the real data given the low statistics in both $p+p$ and
 288 Au+Au samples. In addition, the relative contributions from different Υ states are unknown in Au+Au data. The
 289 number of Υ counts was determined from a direct count of unlike-sign and like-sign dielectrons in the Υ mass region
 290 and the fraction of correlated background f_{cont} in the same mass range. Given the low counts for the signal and
 291 background, Poisson statistics precludes the use of a simple subtraction. Therefore, the Υ signal is determined from

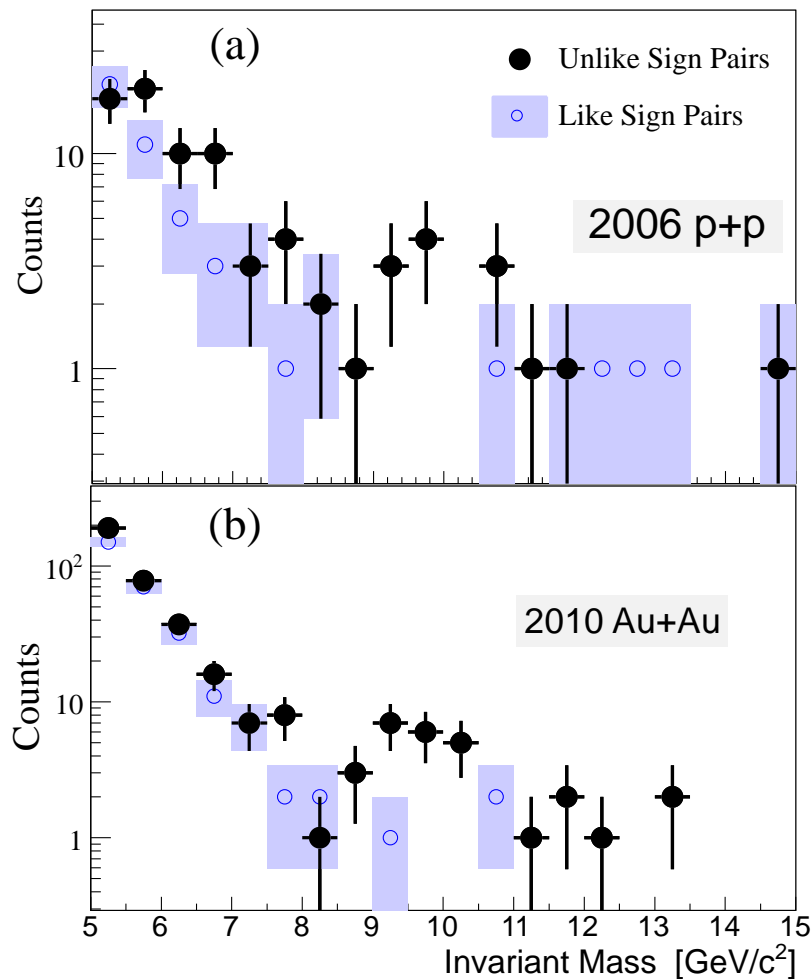


FIG. 5. (Color online) Invariant mass distribution of unlike-sign and like-sign dielectrons in the Υ mass region taken from $p+p$ (a), and Au+Au collisions (b).

$$N_{\Upsilon} = \langle s \rangle_P (1 - f_{\text{cont}}), \quad (1)$$

where $\langle s \rangle_P$ is the average signal from a joint Poisson distribution from the foreground unlike-sign f and background like-sign b dielectron counts in the Υ mass region [57]

$$P(s) = \sum_{k=0}^f \frac{(b+f-k)!}{b!(f-k)!} \frac{1}{2} \left(\frac{1}{2}\right)^{b+f-k} \frac{s^k e^{-s}}{k!}, \quad (2)$$

and the statistical uncertainty corresponds to one standard deviation of the $P(s)$ distribution.

B. Estimation of the continuum contribution

The correlated background underneath the Υ region is determined from fits of the expected mass dependence of Drell-Yan, correlated electrons from B meson decays and possible contamination of hadrons within jets.

The Drell-Yan contribution was estimated from next-to-leading order (NLO) QCD calculations [58]. These calculations are known to reproduce lower and higher energy data at Fermilab [59, 60]. The calculated cross section was used to generate dielectrons propagated through the GEANT [61] based detector simulation. The Drell-Yan contribution is

301 modified by isospin and initial state effects in Au+Au collisions. After calculating the Drell-Yan cross section for $p+n$
 302 and $n+n$ collisions, we found that the Au+Au cross section per binary collision is $f_{\text{iso}} = 89\%$ of that of $p+p$ collisions
 303 because of the isospin effect. The initial state effects were accounted for by using a parton modification factor from
 304 the EPS09 parametrization, $R_q^{DY}(Q^2, x_1, x_2)$, for both Au nuclei. The expected Drell-Yan yield in Au+Au collisions
 305 (Y_{DY}^{AuAu}) relative to the yield in $p+p$ collisions (Y_{DY}^{pp}) is:

$$\frac{Y_{DY}^{\text{AuAu}}(M_{ee})}{N_{\text{coll}}} = Y_{DY}^{pp}(M_{ee}) \cdot f_{\text{iso}} \cdot R_q^{DY}(Q^2, x_1, x_2), \quad (3)$$

306 where N_{coll} is the number of binary collisions. Q^2 , x_1 and x_2 are taken event-by-event from a PYTHIA simulation [62].
 307 Theoretical uncertainties from the NLO calculation, EPS09 quark modification factor ($R_q^{DY}(Q^2, x_1, x_2)$) and overall
 308 detector response were accounted for in the Drell-Yan contribution.

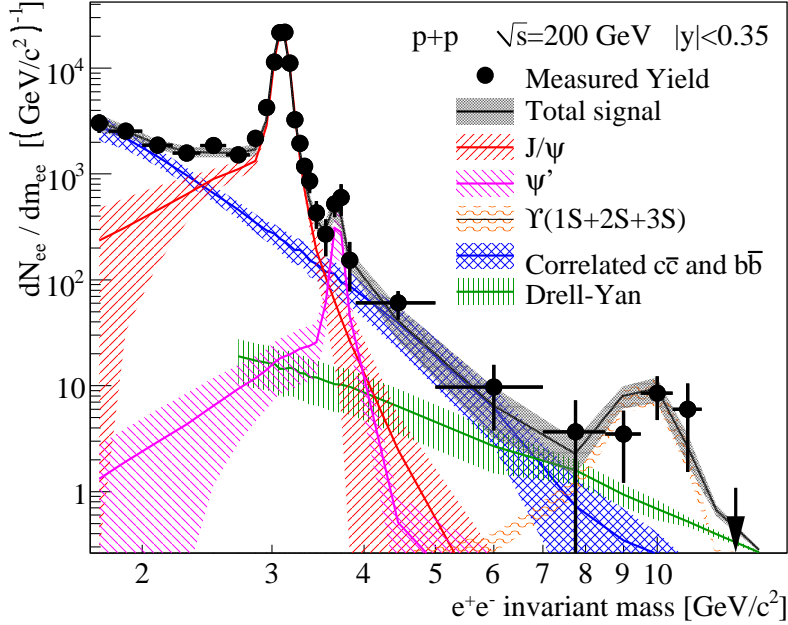


FIG. 6. (Color online) Fitted components to the correlated dielectron mass spectrum in the $p+p$ sample. The bands correspond to the uncertainties obtained from the fit, changes in the heavy flavor generator and theoretical uncertainties in the Drell-Yan contribution.

309 The line shape of the correlated high-mass dielectron distribution from heavy flavor decays in $p+p$ collisions was
 310 studied in detail in [57]. Two approaches were used: (1) a dielectron generator using the measured p_T distribution
 311 of single electrons from heavy flavor with a random opening angle and (2) a heavy flavor simulation from PYTHIA
 312 in the hard scattering mode to emulate NLO contributions. Both generated dielectron distributions were introduced
 313 into the detector simulation and reconstructed like the real data. The mass distribution from heavy flavor decays was
 314 normalized according to a fit to the dielectron spectrum starting at an invariant mass at $1.7 \text{ GeV}/c^2$, thus including
 315 the J/ψ and the ψ' peaks. Figure 6 shows the overall dielectron fit extended to the Υ region. The uncertainty bands
 316 represent the quadratic sum of the fit uncertainties and the differences between the approaches (1) and (2). The
 317 Drell-Yan band represents the quadratic sum of theoretical uncertainties and detector response uncertainties. The
 318 extrapolation of the heavy flavor contribution to the Υ mass range $8.5 < M_{ee}[\text{GeV}/c^2] < 11.5$ in $p+p$ data yields 0.29
 319 ± 0.12 counts, which corresponds to 3.9 ± 1.7 pb. The PYTHIA simulation, including parton shower terms, yields an
 320 estimate that the correlated bottom contribution in this mass range is 3.2 pb, in agreement with the fit extrapolated
 321 result.

322 Jets can contribute to the correlated background in two ways: Dalitz decays from π^0 pairs within the jet and
 323 correlated hadron pair contamination. For a π^0 pair to produce a correlated electron pair in the Υ mass region, each
 324 of the π^0 's should have a transverse momentum larger than the mass of the Υ , which is a possibility ruled out by the
 325 current statistics. Figure 3 shows a not significant hadron contamination in the high-mass dielectrons in $p+p$ data
 326 after combinatorial background subtraction. Hadron contamination was found to be negligible within uncertainties.
 327 Contributions from electron-hadron correlations are also assumed to be negligible.

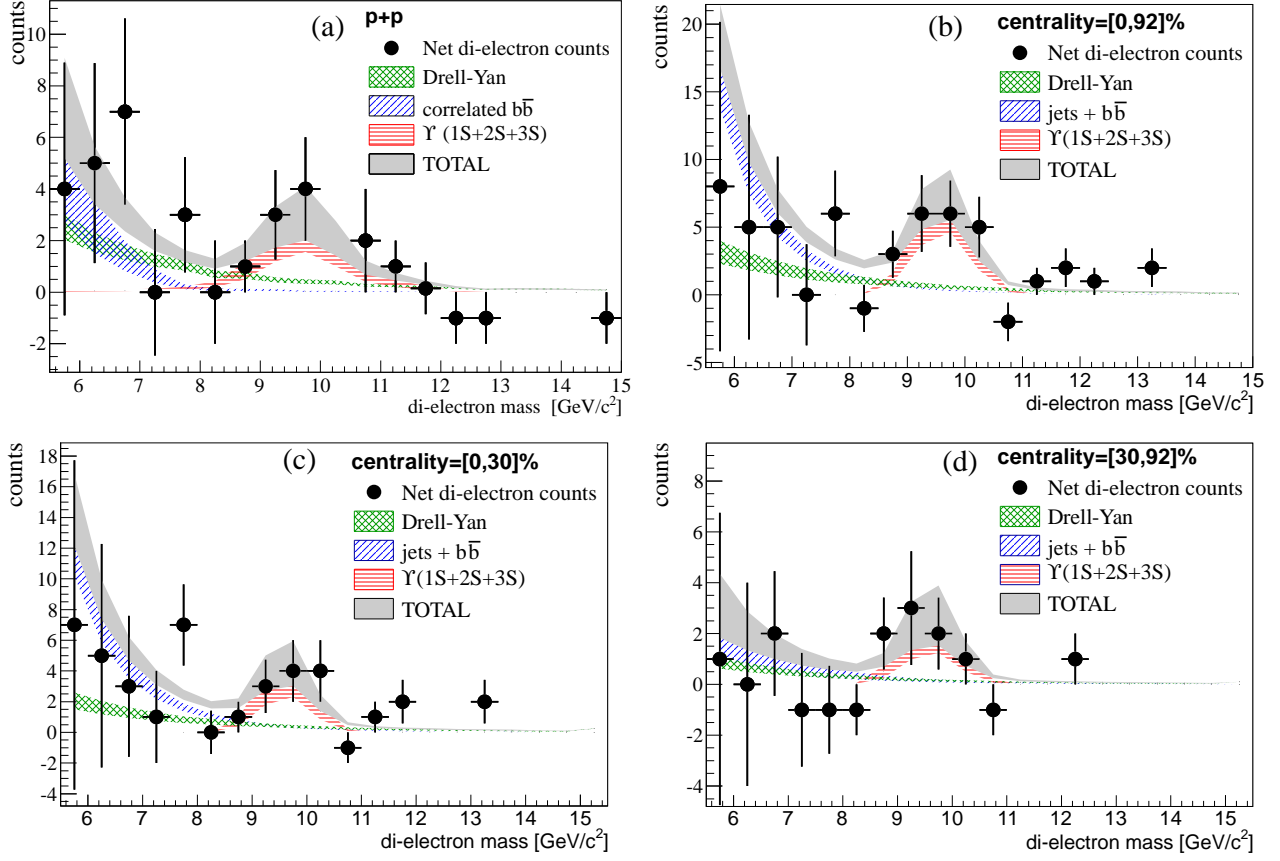


FIG. 7. (Color online) Fits to the correlated dielectron mass distribution around the Υ region obtained in $p+p$ collisions (a) and Au+Au collisions in three centrality bins (b,c,d). The bands correspond to fitting and theoretical uncertainties for the Drell-Yan estimation. Fitting results are used only for correlated background estimations.

328 The resulting continuum fraction in the selected mass range is $f_{\text{cont}}^{pp} = 13 \pm 4\%$ in the $p+p$ sample. The continuum
 329 fraction was also determined with a maximum likelihood fit using the combinatorial background, Drell-Yan, B meson
 330 and Υ line shapes with free parameters for their scales, except the combinatorial background which has a fixed scale.
 331 The total continuum found in this manner was consistent with that estimated with a fixed Drell-Yan scale. The fit
 332 (without any hadron contribution) provides a good description of the mass distribution.

333 We cannot calculate the continuum contributions in Au+Au collisions in the same way as we do for $p+p$ collisions
 334 given the unknown nuclear modification of bottom quarks. Contributions from correlated hadrons may also start to
 335 be significant in a high-occupancy environment. We thus perform a fit to separate the continuum background from
 336 the Υ signal. The dielectron spectrum is described by the following function:

$$\begin{aligned}
 f(m) &= N_{\text{like}} Y_{\text{like}}(m) + Y_{\text{DY}}(m) \\
 &+ N_{\text{bb},\text{jet}} Y_{\text{bb},\text{jet}}(m) + Y_{\Upsilon}(m) \\
 N_{\text{like}} &= \frac{2\sqrt{N_{e^+e^+} + N_{e^-e^-}}}{\int Y_{\text{like}}(m) dm} \\
 N_{\text{bb},\text{jet}} &= \left[N_{\text{cont}} - \int_{m_{\text{low}}}^{m_{\text{high}}} Y_{\text{DY}}(m) dm \right] \\
 Y_{\Upsilon}(m) &= \frac{N_g}{\sqrt{2\pi}\sigma_g} \exp \left[-\frac{1}{2} \left(\frac{m - 9.5}{\sigma_g} \right)^2 \right]
 \end{aligned} \tag{4}$$

337 where $N_{\text{like}} \sim 1$ is the normalization of the like-sign distribution [36], $N_{e^+e^+} + N_{e^-e^-} = 2613$ is the number of like-sign
 338 dielectron pairs over the mass range $5 < M_{ee} [\text{GeV}/c^2] < 15$, $Y_{\text{like}}(m)$ is the like-sign dielectron mass distribution

339 from real data which account for the combinatorial background and a fraction of the correlated background, $Y_{\text{DY}}(m)$
 340 is the Drell-Yan contribution as calculated in Eq. (3), $m_{\text{low}} = 8.5 \text{ GeV}/c^2$ and $m_{\text{high}} = 11.5 \text{ GeV}/c^2$ define the mass
 341 range used in the continuum normalization, N_{cont} is the continuum contribution in the Υ mass region, $Y_{\Upsilon}(m)$ is a
 342 Gaussian function accounting for the Υ peak where σ_g is the effective peak width of all three Υ states combined, and
 343 $Y_{\text{bb},\text{jet}}(m)$ is a function normalized in the Υ mass range which accounts for the correlated open bottom and hadrons
 344 from jets. We assumed both a power law and an exponential function for the correlated bottom and jet contributions:

$$Y_{\text{bb},\text{jet}}(m) = \begin{cases} (\alpha + 1)m^\alpha / (m_{\text{high}}^{\alpha-1} - m_{\text{low}}^{\alpha-1}) \\ \alpha e^{\alpha m} / (e^{\alpha \cdot m_{\text{high}}} - e^{\alpha \cdot m_{\text{low}}}) \end{cases}$$

345 The parameters N_{cont} , α , N_g and σ_g were fit to the unlike-sign dielectron spectrum between 5 and 16 GeV/c^2 using
 346 a maximum likelihood method. Figure 7 shows the $f(m) - N_{\text{like}}Y_{\text{like}}(m)$ fitting result assuming a power law function
 347 for the bottom-jet contribution. The bands represent the fit and theoretical uncertainties. The continuum estimate
 348 changes by up to 0.9% depending on the choice of the bottom+jet contribution function ($Y_{\text{bb},\text{jet}}(m)$). Table III lists
 349 the number of net counts and the continuum fraction for $p+p$ and three centrality ranges in the Au+Au data. The
 350 fraction of continuum in Au+Au data obtained from these fits was found to be larger than in $p+p$ data. This may
 351 reflect that the nuclear modification of Drell-Yan in Au+Au is small compared to the Υ yield modification.

352 C. Mass cut efficiency

353 The Υ count is all made in the mass range $8.5 < M_{\text{ee}}[\text{GeV}/c^2] < 11.5$. The reconstructed Υ family peaks may have
 354 some contribution at masses out of this range. According to the detector simulation using the CDF results [50] for the
 355 relative yields, the mass range $8.5 < M_{\text{ee}}[\text{GeV}/c^2] < 11.5$ contains a fraction $\varepsilon_{\text{mass}} = 0.94 \pm 0.05$ of the $\Upsilon(1S+2S+3S)$
 356 yield in the 2006 $p+p$ data set. The uncertainty of this estimate comes from the mass fit to the $p+p$ data and from
 357 the difference between real data and simulations. In the Au+Au analysis, the evaluation of the detector occupancy
 358 effect on the efficiency included the mass cut used in the analysis. Variations in the detector mass resolution during
 359 this study indicate a systematic uncertainty in the mass cut efficiency of 6% in Au+Au data. The number of Υ counts
 360 has a 2% variation when the normalization of the like-sign dielectrons (N_{like}) is taken from different mass ranges.
 361 This is assigned as a systematic uncertainty on the yield.

362 D. Detector Response

363 The GEANT based detector simulation was tuned as described in [57]. The acceptance and efficiency in this analysis
 364 was obtained from $\Upsilon(1S+2S+3S)$ dielectron decays generated by PYTHIA, requiring that they fall into a rapidity range
 365 of $|y| < 0.5$. The relative yield between Υ states were taken to be those reported by CDF [50]. This same detector
 366 simulation was used to estimate the detector response for the heavy flavor and Drell-Yan background line shapes as
 367 described in the previous section.

368 In the $p+p$ sample, the overall acceptance and efficiency $Acc \times \varepsilon$ for Υ s calculated from simulations was found to
 369 be $(2.33 \pm 0.23) \%$ in the $|y| < 0.5$ rapidity region. The uncertainty of this estimate is from variations in the detector
 370 performance during the run, mismatches between the detector simulation and the detector activity in real data and
 371 variations of the p_T shape introduced in simulation (Fig. 8-a).

372 The BBC trigger samples a cross section of $\sigma_{\text{pp}} \times \varepsilon_{\text{BBC}} = 23 \pm 2.2 \text{ mb}$ in $p+p$ collisions, according to Vernier
 373 scans [64]. However, it samples a larger fraction of the cross section when the collision includes a hard scattering
 374 process. Studies with high p_T π^0 yields showed an increase of the luminosity scanned by the BBC by a factor of
 375 $1/\varepsilon_{\text{BBC}}^{\text{hard}}$, $\varepsilon_{\text{BBC}}^{\text{hard}} = (0.79 \pm 0.02)$ [65]. In Au+Au data the BBC scans $92 \pm 3\%$ of the total Au+Au inelastic cross
 376 section and there is no bias from hard scattering ($\varepsilon_{\text{BBC}}^{\text{hard}}=1$). The EMCAL-RICH trigger (ERT) efficiency of dielectrons
 377 was found to be $(79.6 \pm 3.6)\%$ in the $p+p$ sample when emulating the ERT in MB data. The ERT was not used for
 378 the Au+Au data.

379 In the Au+Au data, the electron identification cuts were tighter, resulting in a calculated acceptance and efficiency
 380 $Acc \times \varepsilon = 1.41 \pm 0.05\%$ (point at 85% centrality in Fig. 9-b). To quantify additional inefficiencies from the detector
 381 occupancy, the raw detector signal from simulated Υ dielectron decays was embedded in real raw data. The simulated
 382 Υ was generated at the same collision point measured in the real event. The reconstruction, fitting and mass cuts of
 383 the embedded data were the same as those used in real data analysis. The p_T and collision centrality dependence of
 384 the resulting fraction of Υ counts in the reconstructed embedded data are shown in Fig. 9. The big difference between

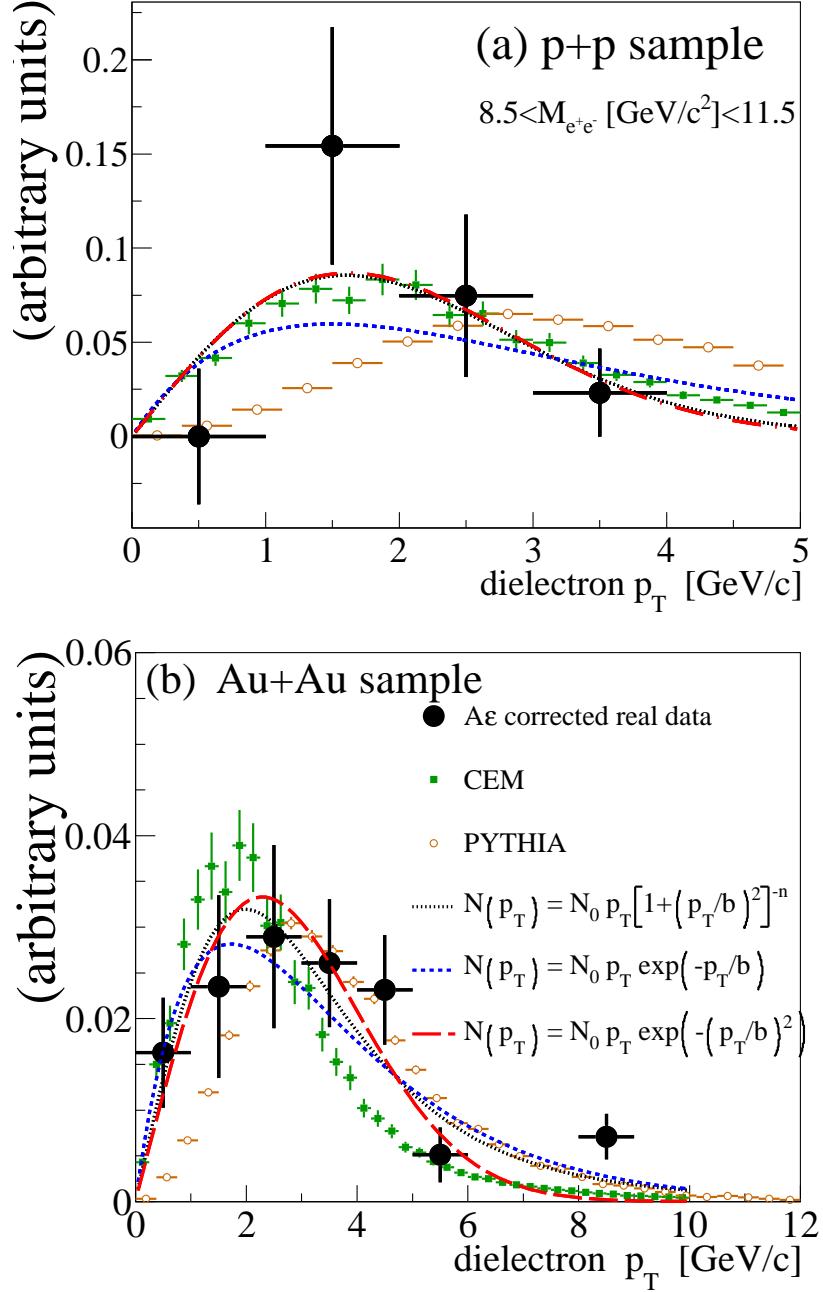


FIG. 8. (Color online) Transverse momentum dependence of acceptance corrected dielectron net counts in the Υ mass region from $p+p$ (a) and centrality integrated Au+Au (b) collisions. The lines are functions and Υ yield estimations (Color Evaporation Model-CEM [63] and PYTHIA [62]) fitted to the distributions.

385 the detector efficiency obtained in $p+p$ data and peripheral Au+Au reflects the tight cuts needed in Au+Au because
 386 of the larger occupancy and additional material in front of the detector in 2010 run.

387 Because we do not have the statistic precision to determine the transverse momentum distribution of the Υ , we
 388 must employ models for the p_T dependence to determine an overall acceptance and efficiency. Five functions were
 389 used for the p_T distribution: a shape from generated Υ decays in PYTHIA, a prediction from the color evaporation
 390 model [63] and three fitted functions $f(p_T)$ to the acceptance corrected real data distribution (Fig. 8). The p_T
 391 integrated acceptance and efficiency is determined by an average using the p_T dependence shown in Fig. 9 and these
 392 functions as weights. The difference between these calculations and the default weighing using PYTHIA as an input is
 393 within 7.8% in $p+p$ and 7.9% in Au+Au samples.

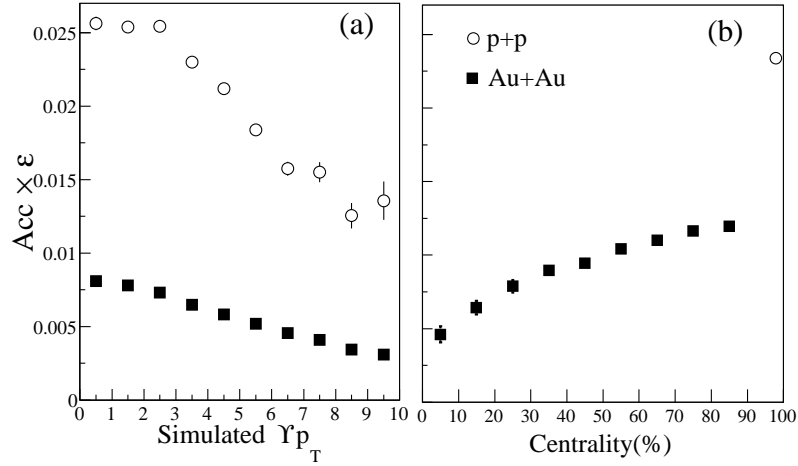


FIG. 9. Dependence of the acceptance \times efficiency for detected Υ dielectron decays in $p+p$ and Au+Au collisions on (a) transverse momentum in 0%–92% centrality and (b) collision centrality. The bars represent statistical uncertainties in the simulation.

TABLE III. Summary of values used in BdN/dy (5) and R_{AA} (7) calculations.

Value	$p+p$	Au+Au 0%–92%	Au+Au 0%–30%	Au+Au 30%–92%
$N_{\text{unlike}} - N_{\text{like}}$	$10.5^{+3.7}_{-3.6}$	$18.3^{+5.0}_{-5.2}$	$11.2^{+3.8}_{-4.0}$	$6.4^{+3.3}_{-3.5}$
f_{cont}	0.13 ± 0.04	0.216 ± 0.045	0.270 ± 0.063	$0.186^{+0.065}_{-0.060}$
$N_{\text{BBC}} \times 10^9$	143	5.40	1.62	3.35
c	0.70	1	1	1
$Acc \times \varepsilon$	$(1.64 \pm 0.25)\%$	$(0.65 \pm 0.13)\%$	$(0.58 \pm 0.11)\%$	$(0.96 \pm 0.18)\%$
N_{coll}	1	258 ± 25	644 ± 63	72 ± 7
N_{part}	2	109 ± 4	242 ± 4	45 ± 2

394 The final values for the efficiency in our wide centrality bins are also sensitive to the true centrality dependence
395 of the Υ production. To estimate this systematic uncertainty we assume two different centrality dependence models:
396 (1) binary collision scaling and (2) participant collision scaling. Within our centrality ranges, we find that these two
397 models yield less than a 7% difference and we include this in our occupancy systematic uncertainty.

398 IV. RESULTS

399 The $\Upsilon \rightarrow e^+e^-$ invariant multiplicity at midrapidity, BdN/dy , is calculated by

$$B \frac{dN}{dy} = \frac{1}{\Delta y} \frac{N_{\Upsilon}}{(N_{\text{BBC}}/c) \cdot Acc \cdot \varepsilon} \quad (5)$$

400 where B is the dielectron branching ratio, N_{Υ} is the number of Υ candidates in the data set as defined in (1), $\Delta y = 1$
401 corresponds to the rapidity range used in simulation (± 0.5), N_{BBC} is the number of analyzed events, $c = \varepsilon_{\text{BBC}}/\varepsilon_{\text{BBC}}^{\text{hard}}$
402 is a correction factor accounting for the limited BBC efficiency and the trigger bias present in events which contain a
403 hard scattering in $p+p$ collisions as explained in Section III D, Acc is the Υ acceptance and ε is the Υ reconstruction
404 efficiency which includes the ERT efficiency. Table III summarizes the numbers used to calculate the Υ yields
405 using Eq. 5. Table IV details the systematic uncertainties involved in the yield calculation. The resulting invariant
406 multiplicities are reported in Table V.

407 The $\Upsilon(1S+2S+3S)$ cross section in $p+p$ collisions is

$$B \frac{d\sigma_{\Upsilon}}{dy} \Big|_{|y| < 0.5} = B \frac{dN}{dy} \times \sigma_{pp} \quad (6)$$

TABLE IV. Summary of the relative systematic uncertainties involved in BdN/dy calculations.

Systematic	Uncertainty	
	$p+p$	Au+Au
acceptance	7.5%	7.0%
electron identification	1.1%	5.0%
simulation input	7.8%	7.9%
mass cut efficiency	6.3%	5.0%
continuum contribution	5%	5.8%–8.6%
acceptance fluctuation	7.3%	14.0%
ERT efficiency	4.5%	NA
occupancy effect	NA	2.0%–7.5%
combinatorial background	2.0%	2.0%
TOTAL	16.1%	20.7-21.2%

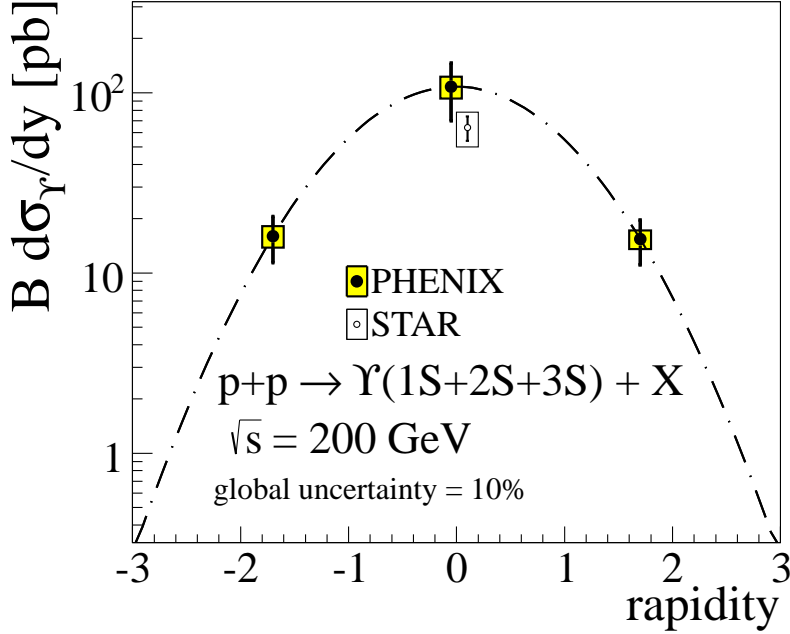


FIG. 10. (Color online) Rapidity dependence of $\Upsilon(1S+2S+3S)$ yield measured by PHENIX, forward rapidity result from [53] and STAR midrapidity from [54]. Dashed line is a Gaussian function fitted to the points. The points at zero rapidity are shifted for clarity.

$$= 108 \pm 38(\text{stat}) \pm 15(\text{syst}) \pm 11(\text{lum}) \text{ pb},$$

408 where $\sigma_{pp} = 42\text{mb}$ is the $p+p$ inelastic cross section at $\sqrt{s} = 200 \text{ GeV}$.

409 Figure 10 shows the rapidity dependence of Υ measured in $p+p$ collisions by PHENIX in the mid- (this analysis),
 410 forward rapidities [53] and the STAR result at midrapidity [54]. Figure 11 presents the collision energy dependence
 411 of the differential cross section at midrapidity along with a NLO calculation using the color evaporation model for
 412 the bottomonium hadronization [63].

413 In addition to the Au+Au 0%–92% centrality sample, we present data in two centrality bins, 0%–30% most central
 414 and 30%–92% most central. Using a Monte Carlo simulation based on the Glauber model in [74], we estimated N_{coll} ,
 415 the average number of binary nucleon-nucleon collisions and N_{part} , the average number of participants, for all data
 416 samples. Figure 12 shows the N_{coll} normalized invariant yield of Υ decays as a function of the number of participants.
 417 For central Au+Au collisions, we observe a reduction of the yield relative to a pure N_{coll} scaling that is typical of
 418 hard scattering processes.

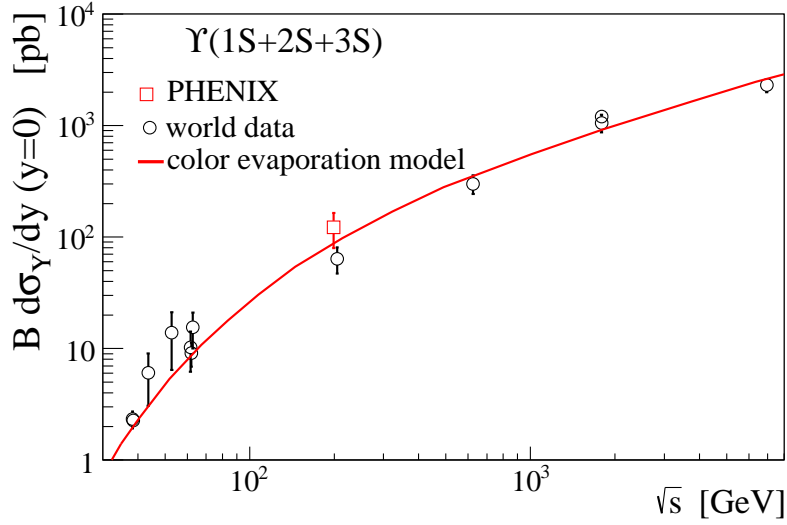


FIG. 11. (Color online) Energy dependence of the $\Upsilon(1S+2S+3S)$ differential cross section at midrapidity in $p+p$ and $p+\bar{p}$ collisions [49, 52, 54, 66–73]. The curve is the estimation using the color evaporation model [63].

TABLE V. Summary of the measured Υ invariant multiplicities, BdN/dy , for one $p+p$ three Au+Au data sets.

Centrality	BdN/dy
$p+p$ ($\times 10^9$)	2.7 ± 0.9 (stat) ± 0.4 (syst)
0%–92% ($\times 10^7$)	$4.1^{+1.1}_{-1.2}$ (stat) ± 0.9 (syst)
0%–30% ($\times 10^7$)	$8.7^{+2.9}_{-3.1}$ (stat) ± 1.8 (syst)
30%–92% ($\times 10^7$)	$1.6^{+0.8}_{-0.9}$ (stat) ± 0.3 (syst)

419 The nuclear modification factors for the binned and integrated 0%–92% centrality data set (R_{AA}) were calculated
420 as:

$$R_{AA} = \frac{dN/dy_{\text{AuAu}}}{\langle N_{\text{coll}} \rangle dN/dy_{pp}} \quad (7)$$

421 and are reported in Table VI. A global uncertainty of 40% is obtained from the quadratic sum of the relative uncer-
422 tainty from 38% $p+p$ data (statistical+systematic) and 12% from the Glauber estimate of the number of collisions.
423 We assume none of the systematic uncertainties are correlated between $p+p$ and Au+Au samples given the different
424 collision environment and changes in the detector configuration between 2006 and 2010 runs, namely active area
425 differences and the installation of the hadron blind detector in 2010 which increased the radiation length from 0.4%
426 to 2.8%.

427 If the $\Upsilon(1S + 2S + 3S)$ yield for Au+Au collisions is equal to the yield for $p+p$ collisions times the number of
428 binary collisions in Au+Au collisions, then $R_{AA} = 1$ and there are no nuclear modification effects. Figure 13 shows
429 the R_{AA} as a function of the number of participants for the two centrality-split classes. The inclusive Υ states are
430 suppressed in central 200 GeV Au+Au collisions, corresponding to large N_{part} . However, the degree of suppression
431 in semi-peripheral collisions is unclear, due to limited statistics.

TABLE VI. Summary of the measured Υ nuclear modification factors, R_{AA} , for Au+Au data sets.

Centrality	R_{AA}
0%–92%	0.58 ± 0.17 (stat) ± 0.13 (syst) ± 0.23 (global)
0%–30%	0.50 ± 0.18 (stat) ± 0.11 (syst) ± 0.20 (global)
30%–92%	$0.84^{+0.45}_{-0.48}$ (stat) ± 0.18 (syst) ± 0.34 (global)

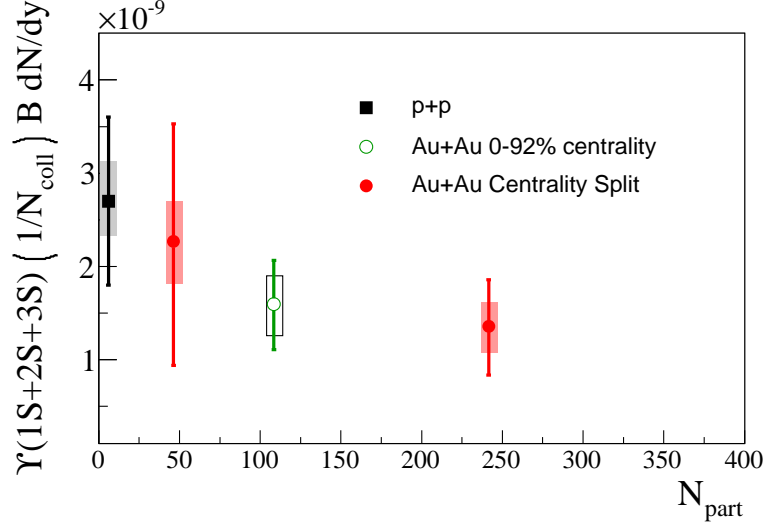


FIG. 12. (Color online) The N_{coll} normalized invariant yield of Υ s produced during the 2006 $p+p$ and the 2010 Au+Au operations, as a function of N_{part} .

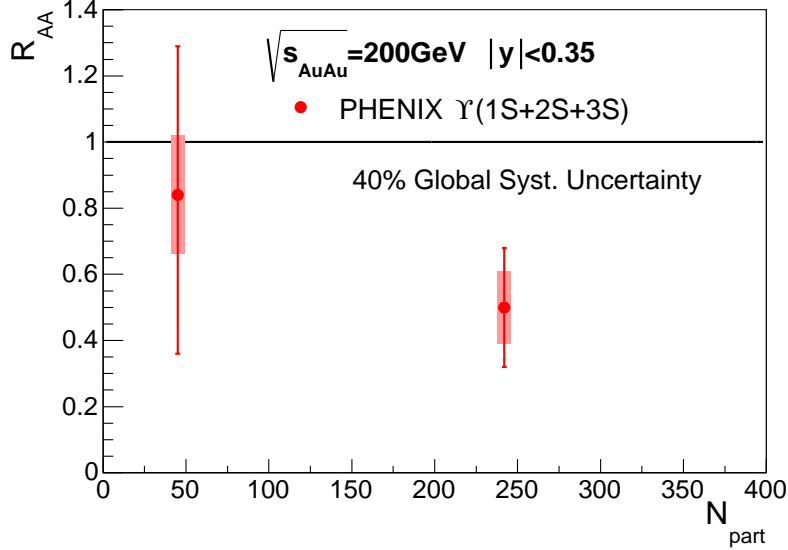


FIG. 13. (Color online) Nuclear modification factor for centrality binned data plotted as a function of N_{part} .

432 In most central events, the suppression is comparable to what is observed in $p(d)+A$ collisions [46, 51–53]. Based
 433 on the lattice calculations discussed before, the bottomonia excited states should be completely dissociated in the
 434 core of Au+Au collisions at RHIC. Table VII summarizes what would be the R_{AA} observed in this study in case the
 435 only nuclear matter effect observed is the complete suppression of these excited states. The estimation is based on
 436 the composition of the Υ states measured and the decays to the $\Upsilon(1S)$ reported in Tables I and II. The R_{AA} obtained
 437 in this analysis is consistent with the suppression of excited states if other initial and final state effects are ignored.

438 The result presented in this work agrees with the STAR experiment at the same energy [54]. The CMS exper-
 439 iment reported centrality dependent nuclear modification factors for the separated $\Upsilon(1S)$ and $\Upsilon(2S)$ states at
 440 $\sqrt{s_{NN}}=2.76$ TeV in Pb+Pb collisions at the LHC [75]. CMS also reported an upper limit of $R_{AA}(\Upsilon(3S))$ of 0.10
 441 at the 95% confidence level. Figure 14 compares the observed inclusive $\Upsilon(1S+2S+3S)$ nuclear modification factor
 442 observed by PHENIX with STAR and the inclusive $\Upsilon(1S+2S)$ measurement by CMS at higher energy showing that
 443 the observed nuclear modification factors are very similar at the two quite different energies.

444 Additionally, it is important to compare the measurements to various model predictions. A model by R. Rapp *et al.*
 445 has frequently been used to interpret J/ψ production [76]. It uses a rate-equation approach, which accounts for both

TABLE VII. $\Upsilon(1S+2S+3S)$ R_{AA} expected when the excited states are completely suppressed in Au+Au collisions along with the measured result in the 30% most central collision regime. Estimations based on Tables I and II.

	R_{AA}
no 2S or 3S	0.65 ± 0.11
no 2S,3S or χ_B	0.37 ± 0.09
measured	0.50 ± 0.18 (stat) ± 0.11 (syst) ± 0.19 (global)

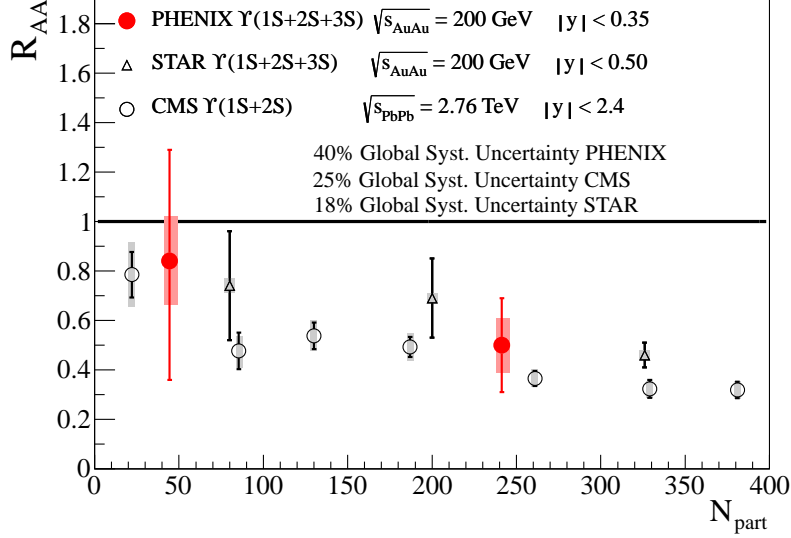


FIG. 14. (Color online) Nuclear modification factor for centrality binned data plotted as a function of N_{part} compared to STAR [54] and CMS results.

446 suppression from cold nuclear matter, color screening of excited states (seen in Fig. 1) and regeneration mechanisms
 447 in the QGP and hadronization phases of the evolving medium. This study looked at two scenarios. The first is
 448 the strong binding scenario where the bottomonium binding energy was not affected by the presence of the QGP,
 449 remaining at the values found in vacuum, and is shown in Fig. 15. The other is the weak binding scenario where the
 450 bottomonium bound-state energies are significantly reduced in the QGP, relative to the vacuum state, adopting the
 451 screened Cornell-potential results of [77] and is shown in Fig. 16. Our data, albeit with large statistical uncertainties,
 452 are consistent with both versions of this model.

453 More recently, two new models were suggested by Strickland and Bazow [78] based on the potential model [77],
 454 with the addition of an anisotropic momentum term. Models A and B are identical, except for an additional term in
 455 Model B which adds an entropy contribution to the free energy. Figure 17 shows the PHENIX measurement along
 456 with the two model predictions, each with a variety of values for the ratio of the shear viscosity to the entropy density.
 457 No definitive statement can be made regarding the shear viscosity. However, the extreme potential B case appears to
 458 be favored.

459 V. CONCLUSIONS

460 In summary, we have studied the production of the sum of Υ states 1S, 2S and 3S at $\sqrt{s_{NN}} = 200$ GeV in the
 461 midrapidity region. The dielectron channel differential cross section in $p+p$ collisions is $Bd\sigma/dy = 108 \pm 38$ (stat)
 462 ± 15 (syst) ± 11 (luminosity) pb. The nuclear modification seen in Au+Au minimum bias collisions is 0.58 ± 0.17
 463 (stat) ± 0.13 (syst) ± 0.23 (global), whereas it is $0.84^{+0.45}_{-0.48}$ (stat) ± 0.18 (syst) ± 0.34 (global) in the mid-peripheral
 464 events and 0.50 ± 0.18 (stat) ± 0.11 (syst) ± 0.20 (global) in the 30% most central events. The nuclear modification
 465 is consistent with the complete suppression of the bottomonium excited states ($\Upsilon(2S)$, $\Upsilon(3S)$ and χ_B), in qualitative
 466 agreement with most calculations as compiled in Fig. 1, assuming no cold nuclear matter effects. There are several
 467 detailed model calculations that show good agreement with our measured modifications. The nuclear modification
 468 factors measured by PHENIX are similar to measurements by STAR at the same energy and by CMS at much higher

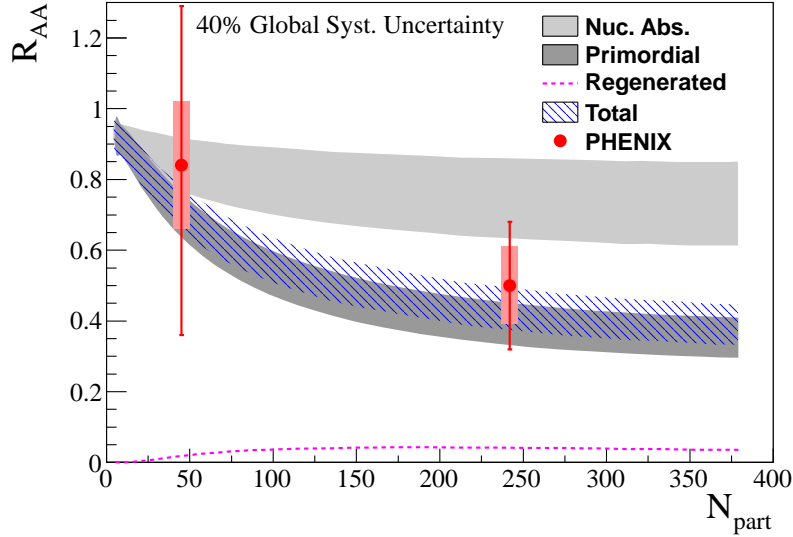


FIG. 15. (Color online) A comparison of PHENIX data to the model from [76] for the strong binding scenario.

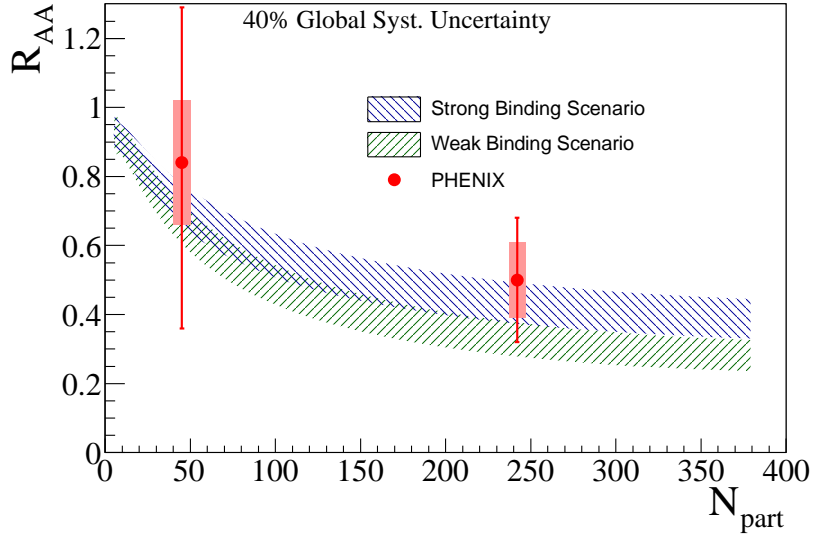


FIG. 16. (Color online) A comparison of PHENIX Υ data to the model from [76] for the weak and strong binding scenario.

469 energy, $\sqrt{s_{NN}}=2.76$ TeV.

470

ACKNOWLEDGMENTS

471 We thank the staff of the Collider-Accelerator and Physics Departments at Brookhaven National Laboratory and
 472 the staff of the other PHENIX participating institutions for their vital contributions. We acknowledge support from
 473 the Office of Nuclear Physics in the Office of Science of the Department of Energy, the National Science Foundation,
 474 a sponsored research grant from Renaissance Technologies LLC, Abilene Christian University Research Council,
 475 Research Foundation of SUNY, and Dean of the College of Arts and Sciences, Vanderbilt University (U.S.A), Ministry
 476 of Education, Culture, Sports, Science, and Technology and the Japan Society for the Promotion of Science (Japan),
 477 Conselho Nacional de Desenvolvimento Científico e Tecnológico and Fundação de Amparo à Pesquisa do Estado de
 478 São Paulo (Brazil), Natural Science Foundation of China (P. R. China), Croatian Science Foundation and Ministry
 479 of Science, Education, and Sports (Croatia), Ministry of Education, Youth and Sports (Czech Republic), Centre

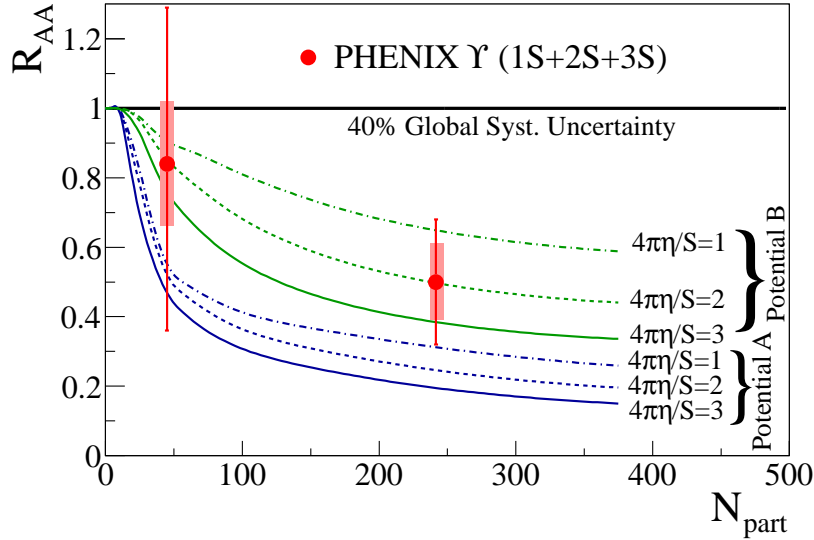


FIG. 17. (Color online) Centrality dependent R_{AA} compared to model predictions from Strickland and Bazow [78] .

480 National de la Recherche Scientifique, Commissariat à l'Énergie Atomique, and Institut National de Physique Nucléaire
 481 et de Physique des Particules (France), Bundesministerium für Bildung und Forschung, Deutscher Akademischer
 482 Austausch Dienst, and Alexander von Humboldt Stiftung (Germany), Hungarian National Science Fund, OTKA, and
 483 the Hungarian American Enterprise Scholarship Fund (Hungary), Department of Atomic Energy and Department of
 484 Science and Technology (India), Israel Science Foundation (Israel), National Research Foundation and WCU program
 485 of the Ministry Education Science and Technology (Korea), Physics Department, Lahore University of Management
 486 Sciences (Pakistan), Ministry of Education and Science, Russian Academy of Sciences, Federal Agency of Atomic
 487 Energy (Russia), VR and Wallenberg Foundation (Sweden), the U.S. Civilian Research and Development Foundation
 488 for the Independent States of the Former Soviet Union, the US-Hungarian Fulbright Foundation for Educational
 489 Exchange, and the US-Israel Binational Science Foundation.

-
- 490 [1] E. Eichten, K. Gottfried, T. Kinoshita, K. D. Lane, and T. M. Yan, "Charmonium: Comparison with experiment," Phys.
 491 Rev. D **21**, 203 (1980).
 492 [2] K. Adcox *et al.* (PHENIX Collaboration), "Formation of dense partonic matter in relativistic nucleus-nucleus collisions at
 493 RHIC: Experimental evaluation by the PHENIX Collaboration," Nucl. Phys. A **757**, 184 (2005).
 494 [3] T. Matsui and H. Satz, "J/psi suppression by quark-gluon plasma formation," Phys. Lett. B **178**, 416 (1986).
 495 [4] Kei Suzuki, Philipp Gubler, Kenji Morita, and Makoto Oka, "Thermal modification of bottomonium spectra from {QCD}
 496 sum rules with the maximum entropy method," Nucl. Phys. A **897**, 28 (2013).
 497 [5] T. Umeda, R. Katayama, O. Miyamura, and H. Matsufuru, "Study of charmonia near the deconfining transition on an
 498 anisotropic lattice with O(a) improved quark action," Int. J. Mod. Phys. A **16**, 2215 (2001).
 499 [6] M. Asakawa and T. Hatsuda, "J / psi and eta(c) in the deconfined plasma from lattice QCD," Phys. Rev. Lett. **92**, 012001
 500 (2004).
 501 [7] Saumen Datta, Frithjof Karsch, Peter Petreczky, and Ines Wetzorke, "Behavior of charmonium systems after deconfinement,"
 502 Phys. Rev. D **69**, 094507 (2004).
 503 [8] A. Jakovac, P. Petreczky, K. Petrov, and A. Velytsky, "Quarkonium correlators and spectral functions at zero and finite
 504 temperature," Phys. Rev. D **75**, 014506 (2007).
 505 [9] Gert Aarts, Chris Allton, Mehmet Bugrahan Oktay, Mike Peardon, and Jon-Ivar Skullerud, "Charmonium at high
 506 temperature in two-flavor QCD," Phys. Rev. D **76**, 094513 (2007).
 507 [10] Alexander Rothkopf, Tetsuo Hatsuda, and Shoichi Sasaki, "Complex Heavy-Quark Potential at Finite Temperature from
 508 Lattice QCD," Phys. Rev. Lett. **108**, 162001 (2012).
 509 [11] G. Aarts, C. Allton, S. Kim, M. P. Lombardo, M. B. Oktay, S. M. Ryan, D. K. Sinclair, and J.-I. Skullerud (FASTSUM
 510 Collaboration), "What happens to the Upsilon and η_b in the quark-gluon plasma? Bottomonium spectral functions from
 511 lattice QCD," (), J. High Energy Phys. **11** (2011), 103.

- [12] G. Aarts, S. Kim, M. P. Lombardo, M. B. Oktay, S. M. Ryan, D. K. Sinclair, and J. I. Skullerud (FASTSUM Collaboration), “Bottomonium above deconfinement in lattice nonrelativistic QCD,” *Phys. Rev. Lett.* **106**, 061602 (2011).
- [13] Gert Aarts, Chris Allton, Seyong Kim, Maria Paola Lombardo, Mehmet B. Oktay, S. M. Ryan, D. K. Sinclair, and J.-I. Skullerud (FASTSUM Collaboration), “S wave bottomonium states moving in a quark-gluon plasma from lattice NRQCD,” *J. High Energy Phys.* **03 (2013)**, 084.
- [14] G. Aarts, C. Allton, S. Kim, M. P. Lombardo, S. M. Ryan, and J.-I. Skullerud (FASTSUM Collaboration), “Melting of P wave bottomonium states in the quark-gluon plasma from lattice NRQCD,” *J. High Energy Phys.* **12 (2013)**, 064.
- [15] F. Karsch, E. Laermann, Swagato Mukherjee, and P. Petreczky, “Signatures of charmonium modification in spatial correlation functions,” *Phys. Rev. D* **85**, 114501 (2012).
- [16] Kenji Morita and Su Houng Lee, “Mass shift and width broadening of J/ψ in QGP from QCD sum rule,” *Phys. Rev. Lett.* **100**, 022301 (2008).
- [17] Kenji Morita and Su Houng Lee, “Critical behavior of charmonia across the phase transition: A QCD sum rule approach,” *Phys. Rev. C* **77**, 064904 (2008).
- [18] Young-Ho Song, Su Houng Lee, and Kenji Morita, “In-medium modification of P-wave charmonia from QCD sum rules,” *Phys. Rev. C* **79**, 014907 (2009).
- [19] Kenji Morita and Su Houng Lee, “Heavy quarkonium correlators at finite temperature: QCD sum rule approach,” *Phys. Rev. D* **82**, 054008 (2010).
- [20] Philipp Gubler, Kenji Morita, and Makoto Oka, “Charmonium spectra at finite temperature from QCD sum rules with the maximum entropy method,” *Phys. Rev. Lett.* **107**, 092003 (2011).
- [21] Youngman Kim, Jong-Phil Lee, and Su Houng Lee, “Heavy quarkonium in a holographic QCD model,” *Phys. Rev. D* **75**, 114008 (2007).
- [22] Mitsutoshi Fujita, Kenji Fukushima, Tatsuhiro Misumi, and Masaki Murata, “Finite-temperature spectral function of the vector mesons in an AdS/QCD model,” *Phys. Rev. D* **80**, 035001 (2009).
- [23] Jorge Noronha and Adrian Dumitru, “Thermal Width of the Υ at Large t' Hooft Coupling,” *Phys. Rev. Lett.* **103**, 152304 (2009).
- [24] Hovhannes R. Grigoryan, Paul M. Hohler, and Mikhail A. Stephanov, “Towards the Gravity Dual of Quarkonium in the Strongly Coupled QCD Plasma,” *Phys. Rev. D* **82**, 026005 (2010).
- [25] M. Laine, “A Resummed perturbative estimate for the quarkonium spectral function in hot QCD,” *J. High Energy Phys.* **05 (2007)**, 028.
- [26] Cheuk-Yin Wong, “Heavy quarkonia in quark-gluon plasma,” *Phys. Rev. C* **72**, 034906 (2005).
- [27] Nora Brambilla, Jacopo Ghiglieri, Antonio Vairo, and Peter Petreczky, “Static quark-antiquark pairs at finite temperature,” *Phys. Rev. D* **78**, 014017 (2008).
- [28] S. Digal, O. Kaczmarek, F. Karsch, and H. Satz, “Heavy quark interactions in finite temperature QCD,” *Eur. Phys. J. C* **43**, 71 (2005).
- [29] W. M. Alberico, A. Beraudo, A. De Pace, and A. Molinari, “Heavy quark bound states above $T(c)$,” *Phys. Rev. D* **72**, 114011 (2005).
- [30] Agnes Mocsy and Peter Petreczky, “Can quarkonia survive deconfinement?” *Phys. Rev. D* **77**, 014501 (2008).
- [31] Agnes Mocsy and Peter Petreczky, “Color screening melts quarkonium,” *Phys. Rev. Lett.* **99**, 211602 (2007).
- [32] Peter Petreczky, Chuan Miao, and Agnes Mocsy, “Quarkonium spectral functions with complex potential,” *Nucl. Phys. A* **855**, 125 (2011).
- [33] D. Cabrera and R. Rapp, “T-Matrix Approach to Quarkonium Correlation Functions in the QGP,” *Phys. Rev. D* **76**, 114506 (2007).
- [34] F. Riek and R. Rapp, “Quarkonia and Heavy-Quark Relaxation Times in the Quark-Gluon Plasma,” *Phys. Rev. C* **82**, 035201 (2010).
- [35] Felix Riek and Ralf Rapp, “Selfconsistent Evaluation of Charm and Charmonium in the Quark-Gluon Plasma,” *New J. Phys.* **13**, 045007 (2011).
- [36] A. Adare *et al.* (PHENIX Collaboration), “Detailed measurement of the e^+e^- pair continuum in $p+p$ and Au+Au collisions at $\sqrt{s_{NN}} = 200$ GeV and implications for direct photon production,” *Phys. Rev. C* **81**, 034911 (2010).
- [37] A. Adare *et al.* (PHENIX Collaboration), “ J/ψ Production versus Centrality, Transverse Momentum, and Rapidity in Au+Au Collisions at $s_{NN} = 200$ GeV,” *Phys. Rev. Lett.* **98**, 232301 (2007).
- [38] A. Adare *et al.* (PHENIX Collaboration), “ J/ψ suppression at forward rapidity in Au+Au collisions at $\sqrt{s_{NN}} = 200$ GeV,” *Phys. Rev. C* **84**, 054912 (2011).
- [39] A. Adare *et al.* (PHENIX Collaboration), “Ground and excited state charmonium production in $p+p$ collisions at $\sqrt{s} = 200$ GeV,” *Phys. Rev. D* **85**, 092004 (2012).
- [40] A. Adare *et al.* (PHENIX Collaboration), “Cold Nuclear Matter Effects on J/ψ Yields as a Function of Rapidity and Nuclear Geometry in $d + A$ Collisions at $\sqrt{s_{NN}} = 200$ GeV,” *Phys. Rev. Lett.* **107**, 142301 (2011).
- [41] A. Adare *et al.* (PHENIX Collaboration), “Transverse-momentum dependence of the J/ψ nuclear modification in $d+Au$ collisions at $\sqrt{s_{NN}} = 200$ GeV,” *Phys. Rev. C* **87**, 034904 (2013).
- [42] A. Adare *et al.* (PHENIX Collaboration), “Measurement of High- p_T Single Electrons from Heavy-Flavor Decays in $p + p$ Collisions at $\sqrt{s} = 200$ GeV,” *Phys. Rev. Lett.* **97**, 252002 (2006).
- [43] Robert L. Thews, Martin Schroedter, and Johann Rafelski, “Enhanced J/ψ production in deconfined quark matter,” *Phys. Rev. C* **63**, 054905 (2001).
- [44] A. Adare *et al.* (PHENIX Collaboration), “Measurement of Bottom versus Charm as a Function of Transverse Momentum with Electron-Hadron Correlations in p^+p Collisions at $\sqrt{s} = 200$ GeV,” *Phys. Rev. Lett.* **103**, 082002 (2009).

- 576 [45] J. Beringer *et al.* (Particle Data Group), “Review of Particle Physics (RPP),” Phys. Rev. D **86**, 010001 (2012).
- 577 [46] L. Y. Zhu *et al.* (FNAL E866/NuSea Collaboration), “Measurement of Υ Production for $p + p$ and $p + d$ Interactions at
578 800 GeV/ c ,” Phys. Rev. Lett. **100**, 062301 (2008).
- 579 [47] F. Abe *et al.* (CDF Collaboration), “ Υ Production in $p\bar{p}$ Collisions at $\sqrt{s} = 1.8$ TeV,” Phys. Rev. Lett. **75**, 4358 (1995).
- 580 [48] R. Aaij *et al.* (LHCb Collaboration), “Measurement of Upsilon production in pp collisions at $\sqrt{s} = 7$ TeV,” Eur. Phys. J.
581 C **72**, 2025 (2012).
- 582 [49] Vardan Khachatryan *et al.* (CMS Collaboration), “Measurement of the Inclusive Υ production cross section in pp collisions
583 at $\sqrt{s} = 7$ TeV,” Phys. Rev. D **83**, 112004 (2011).
- 584 [50] T. Affolder *et al.* (CDF Collaboration), “Production of ΥS Mesons from χ_b Decays in $p\bar{p}$ Collisions at $\sqrt{s} = 1.8$ TeV,”
585 Phys. Rev. Lett. **84**, 2094 (2000).
- 586 [51] D. M. Alde *et al.*, “Nuclear dependence of the production of Υ resonances at 800 GeV,” Phys. Rev. Lett. **66**, 2285 (1991).
- 587 [52] G. Moreno *et al.*, “Dimuon production in proton-copper collisions at $\sqrt{s} = 38.8$ GeV,” Phys. Rev. D **43**, 2815 (1991).
- 588 [53] A. Adare *et al.* (PHENIX Collaboration), “ $\Upsilon(1S+2S+3S)$ production in $d+Au$ and $p + p$ collisions at $\sqrt{s_{NN}} = 200$ GeV
589 and cold-nuclear-matter effects,” Phys. Rev. C **87**, 044909 (2013).
- 590 [54] L. and others Adamczyk (STAR Collaboration), “Suppression of v production in $d+au$ and $au+au$ collisions at $\sqrt{s_{NN}} = 200$
591 gev,” Phys. Lett. B **735**, 127 (2014).
- 592 [55] S. Chatrchyan *et al.* (CMS Collaboration), “Observation of Sequential Υ Suppression in PbPb Collisions,” Phys. Rev. Lett.
593 **109**, 222301 (2012).
- 594 [56] K. Adcox *et al.* (PHENIX Collaboration), “PHENIX central arm tracking detectors,” Nucl. Instrum. Methods Phys. Res.,
595 Sect. A **499**, 489 (2003).
- 596 [57] A. Adare *et al.* (PHENIX Collaboration), “Ground and excited charmonium state production in $p+p$ collisions at $\sqrt{s} = 200$
597 GeV,” Phys. Rev. D **85**, 092004 (2012).
- 598 [58] J. Kubar, M. Le Bellac, J. L. Meunier, and G. Plaut, “QCD Corrections to the Drell-Yan Mechanism and the Pion
599 Structure Function,” Nucl. Phys. B **175**, 251 (1980).
- 600 [59] J.C. Webb *et al.* (NuSea Collaboration), “Absolute Drell-Yan dimuon cross-sections in 800 GeV/ c pp and pd collisions,”
601 ArXiv:hep-ex/0302019.
- 602 [60] T. Affolder *et al.* (CDF Collaboration), “Measurement of $d\sigma/dy$ for high mass Drell-Yan e^+e^- pairs from $p\bar{p}$ collisions at
603 $\sqrt{s} = 1.8$ TeV,” Phys. Rev. D **63**, 011101 (2000).
- 604 [61] *GEANT 3.2.1*, GEANT 3.2.1, CERN Program Library (1993), <http://wwwasdoc.web.cern.ch/wwwasdoc/pdfdir/geant.pdf>.
605
- 606 [62] Torbjorn Sjostrand, Stephen Mrenna, and Peter Skands, “PYTHIA 6.4 Physics and Manual,” J. High Energy Phys. **05**
607 (2006), 026.
- 608 [63] R. E. Nelson, R. Vogt, and A. D. Frawley, “Narrowing the uncertainty on the total charm cross section and its effect on
609 the J/ψ cross section,” Phys. Rev. C **87**, 014908 (2013).
- 610 [64] S. S. Adler *et al.*, “Midrapidity Neutral-Pion Production in Proton-Proton Collisions at $\sqrt{s} = 200$ GeV,” Phys. Rev. Lett.
611 **91**, 241803 (2003).
- 612 [65] A. Adare *et al.* (PHENIX Collaboration), “Heavy Quark Production in $p + p$ and Energy Loss and Flow of Heavy Quarks
613 in Au+Au Collisions at $\sqrt{s_{NN}} = 200$ GeV,” Phys. Rev. C **84**, 044905 (2011).
- 614 [66] J. K. Yoh *et al.*, “Study of Scaling in Hadronic Production of Dimuons,” Phys. Rev. Lett. **41**, 684 (1978).
- 615 [67] K. Ueno *et al.*, “Evidence for the Υ' and a Search for New Narrow Resonances,” Phys. Rev. Lett. **42**, 486 (1979).
- 616 [68] S. Childress *et al.*, “Production Dynamics of the Υ in Proton-Nucleon Interactions,” Phys. Rev. Lett. **55**, 1962 (1985).
- 617 [69] T. Yoshida *et al.*, “High-resolution measurement of massive-dielectron production in 800-GeV proton-beryllium collisions,”
618 Phys. Rev. D **39**, 3516 (1989).
- 619 [70] C. Kourkoumelis, L. Resvanis, T. A. Filippas, E. Fokitis, A. M. Cnops, *et al.*, “Characteristics of J/psi and Upsilon
620 production at the CERN intersecting storage rings,” Phys. Lett. B **91**, 481 (1980).
- 621 [71] A. L. S. Angelis *et al.* (CERN-Columbia-Oxford-Rockefeller Collaboration, CCOR Collaboration), “A Measurement of the
622 Production of Massive e^+e^- Pairs in Proton Proton Collisions at $\sqrt{s} = 62.4$ -GeV,” Phys. Lett. B **87**, 398 (1979).
- 623 [72] C. Albajar *et al.* (UA1 Collaboration), “Beauty Production at the CERN Proton- anti-Proton Collider. 1.” Phys. Lett. B
624 **186**, 237 (1987).
- 625 [73] D. Acosta *et al.* (CDF Collaboration), “ Υ production and polarization in $p\bar{p}$ collisions at $\sqrt{s} = 1.8$ -TeV,” Phys. Rev. Lett.
626 **88**, 161802 (2002).
- 627 [74] Michael L. Miller, Klaus Reygers, Stephen J. Sanders, and Peter Steinberg, “Glauber modeling in high energy nuclear
628 collisions,” Ann. Rev. Nucl. Part. Sci. **57**, 205 (2007).
- 629 [75] Serguei Chatrchyan *et al.* (CMS Collaboration), “Observation of sequential Upsilon suppression in PbPb collisions,” Phys.
630 Rev. Lett. **109**, 222301 (2012).
- 631 [76] A. Emerick, X. Zhao, and R. Rapp, “Bottomonia in the Quark-Gluon Plasma and their Production at RHIC and LHC,”
632 Eur. Phys. J. A **48**, 72 (2012).
- 633 [77] F. Karsch, M. T. Mehr, and H. Satz, “Color Screening and Deconfinement for Bound States of Heavy Quarks,” Z. Phys.
634 C **37**, 617 (1988).
- 635 [78] Michael Strickland and Dennis Bazow, “Thermal Bottomonium Suppression at RHIC and LHC,” Nucl. Phys. A **879**, 25
636 (2012).